DOE/NASA/0340-1
NASA CR-174971

A Computer Simulation of the Turbocharged Turbocompounded Diesel Engine System: A Description of the Thermodynamic and Heat Transfer Models

Dennis N. Assanis, Jack E. Ekchian,
Rick M. Frank, and John B. Heywood
Sloan Automotive Laboratory
Massachusetts Institute of Technology

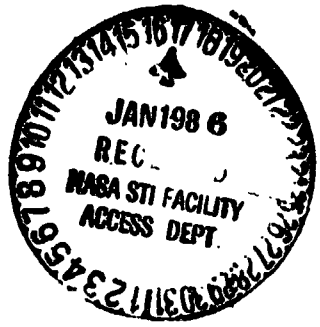

August 1985

Prepared for
NATIONAL AERONAUTICS AND SPACE ADMINISTRATION
Lewis Research Center
Under Grant NAG 3-340

for
U.S. DEPARTMENT OF ENERGY
Conservation and Renewable Energy
Office of Vehicle and Engine R&D

DOE/NASA/0340-1
NASA CR-174971

A Computer Simulation of the Turbocharged Turbocompounded Diesel Engine System: A Description of the Thermodynamic and Heat Transfer Models

Dennis N. Assanis, Jack E. Ekchian,
Rick M. Frank, and John B. Heywood
Sloan Automotive Laboratory
Massachusetts Institute of Technology
Cambridge, Massachusetts 02139

August 1985

Prepared for
National Aeronautics and Space Administration
Lewis Research Center
Cleveland, Ohio 44135
Under Grant NAG 3-340

for
U.S. DEPARTMENT OF ENERGY
Conservation and Renewable Energy
Office of Vechicle and Engine R&D
Washington, D.C. 20545
Under Interagency Agreement DE-AI01-80CS50194

Table of Contents

1. INTRODUCTION

The use of ceramics in heavy duty diesel engine applications is especially promising [1]. It has been shown in the TACOM/Cummins Adiabatic Engine Program that reductions in heat losses at appropriate points in the diesel engine system result in substantially increased exhaust enthalpy [2]. One of the most promising concepts for taking advantage of this increased exhaust enthalpy is the turbocharged turbocompounded diesel engine cycle [3].

This engine concept consists of several sub-systems: compressor, reciprocator, turbocharger turbine, compounded turbine, ducting and heat exchangers. Opportunities for use of ceramic materials in the different sub-system components have widely different degrees of difficulty and benefits. Therefore, there is a need for a computer simulation of this complete engine concept, at the appropriate level of detail, to enable engineers to define the trade-offs associated with introducing ceramic materials in various parts of the total engine system, and to carry out system performance and optimization studies.

This report describes the thermodynamic and heat transfer models used in a computer program which simulates the behavior of the total engine system. The focus of this total system simulation is to define the mass flows and energy transfers (heat transfers, heat release, work transfers) in each sub-system and the relationship between the sub-systems. Since this system model must function as a single-unit, a deliberate effort is made to maintain a balance in the complexity of the various sub-system descriptions.

This effort has been funded by DOE over a two year period. A Phase I computer simulation of the turbocompounded engine system was developed during the first year. The mathematical models used in the Phase I simulation are described in NASA Contractors Report CR-174755 [4]. In order to make the

Phase I program available as quickly as possible, relative simple heat transfer and conduction models were used for the major system components. A validation of this Phase I simulation against data from a turbocompounded engine system was successfully carried out and has also been reported [5]. In the second phase of this program, a substantial extension and upgrading of critical sub-system models was carried out. Major areas of focus were: description of turbomachinery component performance; heat conduction through the piston, cylinder-head, cylinder-liner, exhaust port, exhaust manifold and ducting to incorporate material properties and wall designs appropriate to use of ceramics; radiation from the combustion gases; flow through the exhaust system. The present report describes the models used to represent the mass flow rates, heat transfers to and through the walls, work transfers, energy release in the combustion process, and thermodynamics of the working fluids properties and processes in this Phase II version of the turbocompounded diesel simulation.

Figure 1 illustrates the overall model structure. The air flow is followed through an air filter, ducting, turbocharger compressor, ducting, cooler and engine intake system to the diesel reciprocator. The reciprocator simulation is a mathematical model of the processes occurring in the direct-injection four-stroke diesel-engine. Engine friction sub-models are then used to obtain brake quantities from the computed reciprocator indicated performance quantities. The exhaust gas flow is followed through the engine exhaust ports, manifold runners and plenum, to the turbocharger turbine; it is then followed through additional ducting to the compounded turbine; the flow then passes through the exhaust system and muffler to the atmosphere.

The report is arranged as follows. First, the basic assumptions of the reciprocator and the other component models are summarized. Then, the

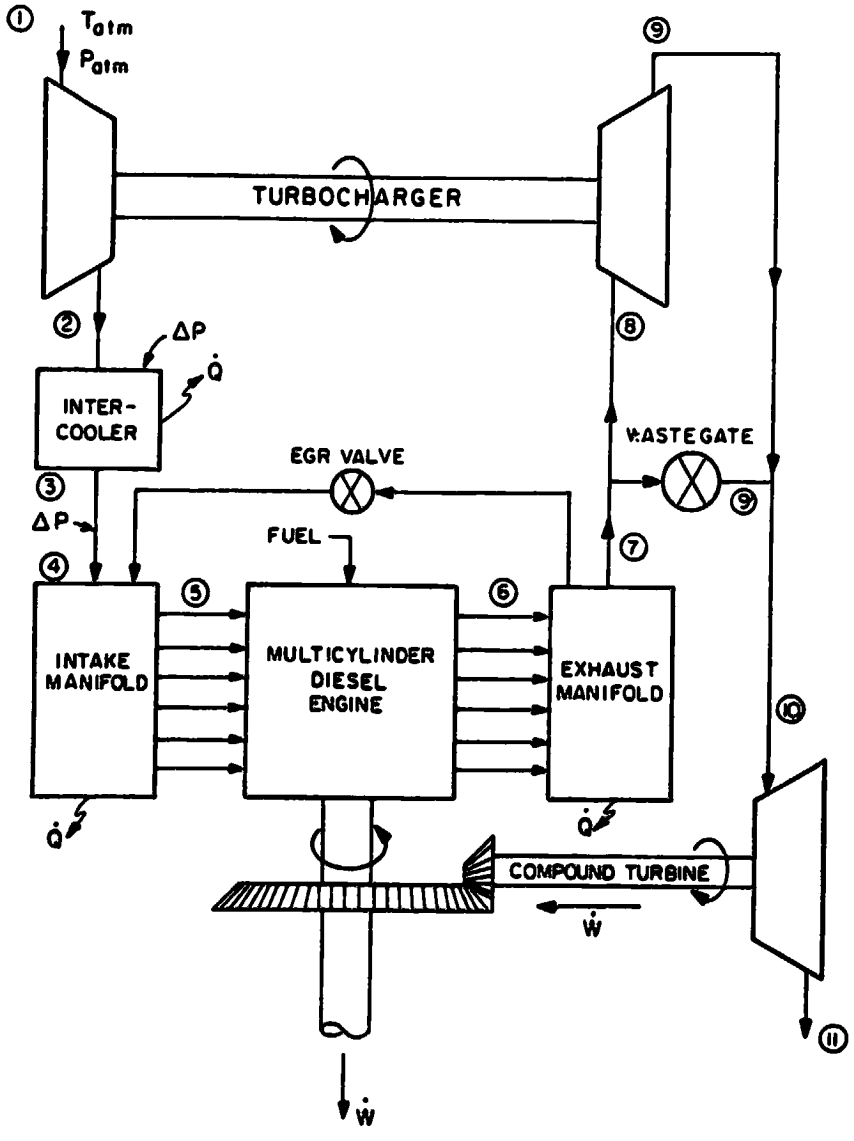

Fig. 1: Turbocompounded diesel system configuration.

mathematical relationships for mass and energy conservation for an open system (such as the manifolds and engine cylinder) are developed. Then, the models which represent each process in the individual components of the total system are described. Next, the method of solution of the complete model that results from the integration of the various sub-systems is presented, along with a typical set of program inputs and outputs.

2. BASIC ASSUMPTIONS OF SYSTEM MODELS

2.1 Reciprocator Engine Model

The diesel four-stroke cycle is treated as a sequence of continuous processes: intake, compression, combustion (including expansion), and exhaust. The durations of the individual processes are as follows. The intake process begins when the intake valve opens (IVO) and ends when the intake valve closes (IVC). The compression process begins at IVC and ends at the time of ignition (IGN). The combustion process begins when ignition occurs and ends when the exhaust valve opens (EVO). The exhaust process begins at EVO and ends at IVO (and not when the exhaust valve closes).

In the reciprocator simulation, the system of interest is the instantaneous contents of a cylinder, i.e. air, fuel and combustion products. In general, this system is open to the transfer of mass, enthalpy, and energy in the form of work and heat. Throughout the cycle, the cylinder is treated as a variable volume plenum, spatially uniform in pressure. Furthermore, the cylinder contents are represented as one continuous medium by defining an average equivalence ratio and temperature in the cylinder at all times.

Gas properties are calculated assuming ideal gas behavior. At low temperatures (below 1000 K), the cylinder contents are treated as a homogeneous mixture of non-reacting ideal gases. At high temperatures (above 1000 K), the properties of the cylinder contents are calculated with allowance for chemical dissociation by assuming that the burned gases are in equilibrium, using an approximate calculation method based on hydrocarbon-air combustion.

Quasi-steady, adiabatic, one-dimensional flow equations are used to predict mass flows past the intake and exhaust valves. The intake manifold and the exhaust port are treated as plenums whose pressure and temperature

history is determined by solution of the manifold state equations. When reverse flow past the intake valve occurs, rapid mixing of the back flow gases within the intake manifold is assumed.

The compression process is defined so as to include the ignition delay period, i.e. the time interval between the start of the injection process (the point at which the injector needle starts to lift) and the ignition point (the start of positive heat release due to combustion). The total length of the ignition delay is related to the mean cylinder gas temperature and pressure during the delay period by an empirical Arrhenius expression.

Combustion is modelled as a uniformly distributed heat release process. The rate of heat release is assumed to be proportional to the rate of fuel burning which is modelled empirically. Since the diesel combustion process is comprised of a pre-mixed and a diffusion-controlled combustion mechanism, Watson's fuel burning rate correlation [6], consisting of the sum of two algebraic functions, one for each combustion mechanism, is used. The fraction of the total fuel injected that is burnt by either mechanism depends on the length of the ignition delay period and the engine load and speed.

Heat transfer is included in all the engine processes. Convective heat transfer is modelled using available engine correlations based on turbulent flow in pipes. The characteristic velocity and length scales required to evaluate these correlations are obtained from a mean and turbulent kinetic energy model. Radiative heat transfer is added during combustion. The steady-state inside wall surface temperatures of the piston, cylinder head, and liner can be either specified or calculated from a specification of the component wall structure. Additionally, the time-dependent temperature distribution in the piston and cylinder head can be computed using a one-dimensional finite difference model.

Finally, an empirical friction model is used to convert the indicated engine performance quantities to brake performance quantities.

2.2 Other Component Models

The reciprocator engine model calculates the state variables in one master cylinder of a multi-cylinder engine, while the manifolds and the other component models have inherent multi-cylinder capability. The interaction between the master cylinder model and the other components is accounted for in the manifolds. To simulate the effect of additional cylinders on the manifold conditions, and hence on the entire system behavior, the conditions in the other cylinders are assumed to vary as echoes of the master cylinder, shifted by the appropriate phase angles. The following additional assumptions are made in order to develop models for the various components of the complete turbocharged turbocompounded diesel engine system:

Intake air and exhaust gas can be modelled as ideal gases. There is perfect and instantaneous mixing of all mass flows that enter each manifold (or section of the manifold) with the gases in the manifold. This implies that there is no spatial variation in properties within a manifold (or manifold section) at any instant of time, and all flows leaving a manifold have the properties of the manifold (or manifold section) contents. The connecting pipes to and from the intake manifold are included as parts of the intake manifold. The exhaust manifold is modeled as a series of connected open systems: exhaust port, manifold runner and manifold plenum.

There is instantaneous mixing of all mass flows that enter the intake manifold with the gases in the manifold; thus there is no variation in properties within the intake manifold at any instant of time. All flows leaving the intake manifold have the properties of the manifold contents. Similarly, the gas properties are assumed to be uniform within each individual section of the exhaust manifold at any instant of time and the flow out of any section has the properties of that section.

There are no mass transfers except along the routes indicated; i.e., there are no losses or leakages from any component of the system. The flow through the wastegate can be specified as a fraction of the exhaust gas stream. The two exhaust gas streams, through and bypassing the turbocharger turbine, reunite with no loss of thermal energy, at the turbocharger turbine exit pressure. An open-system duct model connects the turbocharger turbine and compounded turbine.

The steady-state inside wall surface temperatures of the manifold sections and ducting can be specified or calculated from wall design information. Empirical correlations are used to calculate instantaneous heat transfer rates from the gas to the walls and pressure losses. Conduction through the walls is modeled as axisymmetric. The boundary conditions on the outside wall surface of each component are specified. From these, the steady-state temperature distribution within the walls of each component can be calculated.

The turbomachinery performance is defined by maps that interrelate efficiency, pressure ratio, mass flow rate and shaft speed for each component. The compressor, turbine, and power turbine are assumed to be adiabatic, i.e., there is no heat transfer from these components to the environment. The turbocharger dynamics are controlled by the rotor inertia and damping. The turbocharger turbine and compressor speeds are equal. Finally, the power turbine shaft is connected to the engine crankshaft via a specified gear ratio transmission. Hence, the power turbine speed can be determined directly from the reciprocator engine speed.

3. CONSERVATION EQUATIONS

In this section, equations for the conservation of mass and energy are developed for the contents of an open thermodynamic system. The conservation equation for the fuel mass is used to develop a differential equation for the change in fuel-air equivalence ratio of the system. The energy conservation equation is developed to obtain a differential equation for the change in temperature of the thermodynamic system.

3.1 Conservation of Mass

3.1.1 Conservation of total mass

The rate of change of the total mass in any open system is equal to the sum of the mass flow rates into and out of the system:

$$\dot{m} = \sum_j \dot{m}_j \qquad (3\text{-}1)$$

Note that the convention used in our model assumes that mass flow rates into the open system are taken as positive, while mass flow rates out of the system are negative.

3.1.2 Conservation of fuel mass

In particular, conservation of the fuel species can be expressed as

$$\dot{m}_f = \sum_j \dot{m}_{f,j} \qquad (3\text{-}2)$$

where m_f denotes the fuel content in the open system (includes fuel added by injection and fuel in the form of combustion products).

Defining the fuel fraction, F, in the system as

$$F = m_f/m$$

where m is the total mass in the system, equation (3-2) can be re-written as

$$\frac{d}{dt}(mF) = \sum_j \dot{m}_j F_j \tag{3-3}$$

where F_j denotes the fuel fraction of the mass flow entering or leaving the open system through the j port.

Differentiating the left-hand side of equation (3-3) gives

$$\dot{m}F = \sum_j \dot{m}_j F_j - \dot{m}F \tag{3-4}$$

or substituting for $\dot{m}$ from equation (3-1) results in a differential equation for the change in the fuel fraction of the open system, i.e.

$$\dot{F} = \sum_j (\dot{m}_j/m)(F_j - F) \tag{3-5}$$

An average fuel-air equivalence ratio, ϕ, for the contents of the open system can be defined as

$$\phi = \frac{m_f/m_a}{FASTO} \tag{3-6}$$

where m_a is the mass of air in the open system and FASTO denotes the stoichiometric fuel to air ratio.

Expressing the equivalence ratio, ϕ, in terms of the fuel fraction, F, i.e.

$$\phi = \frac{1}{FASTO}\,\frac{F}{1-F} \tag{3-7}$$

and differentiating (3-7) with respect to time we obtain an equation for the rate of change of the equivalence ratio of the open system, i.e.

$$\dot{\phi} = \frac{1}{FASTO}\,\frac{\dot{F}}{(1-F)^2} \tag{3-8}$$

with $\dot{F}$ given from equation (3-5).

3.2 Conservation of Energy

The general energy equation for an open thermodynamic system may be written as

$$\dot{E} = \sum_j \dot{m}_j h_j - \dot{Q}_w - \dot{W} \qquad (3\text{-}9)$$

with the rate of change of the energy of the system being given by

$$\dot{E} = \frac{d}{dt}(mh) - \frac{d}{dt}(pV) \qquad (3\text{-}10)$$

where

$\sum_j \dot{m}_j h_j$ is the net rate of influx of enthalpy

$\dot{Q}_w = \sum_i \dot{Q}_i$ is the total heat transfer to the walls, i.e. the sum of the heat transfer rates to the different surfaces of the control volume of interest

$\dot{W} = p\dot{V}$ is the rate at which the system does work by boundary displacement.

The dots denote differentiation with respect to time. Note that the convention used is that heat loss from the system and work done by the system are taken as positive.

Differentiating the left-hand side of equation (3-9) gives

$$\dot{mh} = \sum_j \dot{m}_j h_j - \dot{Q}_w + \dot{pV} - \dot{mh} \qquad (3\text{-}11)$$

The contents of any open system, i.e. air and combustion products, can be represented as one continuous medium by defining an average equivalence ratio at each point in time. Gas properties are obtained assuming ideal gas

behavior and thermodynamic equilibrium (see Appendix A). With these assumptions, we can express the enthalpy, h, and the density, ρ, of the mixture of air and combustion products as

$$h = h(T,p,\phi) \tag{3-12}$$

$$\rho = \rho(T,p,\phi) \tag{3-13}$$

Hence, the rate of change of the above fluid properties with respect to time, or crank-angle, can be written as

$$\dot{h} = c_p \dot{T} + c_T \dot{p} + c_\phi \dot{\phi} \tag{3-14}$$

where

$$c_p = \left(\frac{\partial h}{\partial T}\right)_{p,\phi}$$

$$c_T = \left(\frac{\partial h}{\partial p}\right)_{T,\phi}$$

$$c_\phi = \left(\frac{\partial h}{\partial \phi}\right)_{T,p}$$

and

$$\dot{\rho} = \left(\frac{\partial \rho}{\partial T}\right)_{p,\phi} \dot{T} + \left(\frac{\partial \rho}{\partial p}\right)_{T,\phi} \dot{p} + \left(\frac{\partial \rho}{\partial \phi}\right)_{T,p} \dot{\phi} \tag{3-15}$$

The equation of state for ideal gases

$$p = R\rho T \tag{3-16}$$

can be expressed in differential form as

$$\frac{\dot{p}}{p} = \frac{\dot{R}}{R} + \frac{\dot{\rho}}{\rho} + \frac{\dot{T}}{T} \tag{3-17}$$

Re-arranging equation (3-17) and using (3-16), we can write

$$\dot{R} = \frac{1}{\rho T}\dot{p} - \frac{p}{\rho^2 T}\dot{\rho} - \frac{p}{\rho T^2}\dot{T} \tag{3-18}$$

Substituting for $\dot{\rho}$ from equation (3-15) into the above equation, we can

express $\dot{R}$ in terms of $\dot{p}$, $\dot{T}$ and $\dot{\phi}$, i.e.

$$\dot{R} = \left(\frac{1}{\rho T} - \frac{p}{\rho^2 T}\frac{\partial \rho}{\partial p}\right)\dot{p} - \left(\frac{p}{\rho T^2} + \frac{p}{\rho^2 T}\frac{\partial \rho}{\partial T}\right)\dot{T} - \frac{p}{\rho^2 T}\frac{\partial \rho}{\partial \phi}\dot{\phi} \tag{3-19}$$

From the differential form of the equation of state, we can express the time rate of change of pressure as

$$\dot{p} = p\left(\frac{\dot{R}}{R} + \frac{\dot{m}}{m} + \frac{\dot{T}}{T} - \frac{\dot{V}}{V}\right) \tag{3-20}$$

or substituting for $\dot{R}$ from equation (3-19), and with some manipulation, we obtain the time rate of change of pressure:

$$\dot{p} = \frac{\rho}{\partial \rho / \partial p}\left(-\frac{\dot{V}}{V} - \frac{1}{\rho}\frac{\partial \rho}{\partial T}\dot{T} - \frac{1}{\rho}\frac{\partial \rho}{\partial \phi}\dot{\phi} + \frac{\dot{m}}{m}\right) \tag{3-21}$$

Returning to the energy equation (3-11), and expressing $\dot{h}$ in terms of its partial derivatives with respect to T, p and ϕ, we obtain

$$mc_p\dot{T} = \sum_j \dot{m}_j h_j - \dot{Q}_w + (V - mc_T)\dot{p} - mc_\phi\dot{\phi} - h\dot{m} \tag{3-22}$$

Finally, substituting for $\dot{p}$ from equation (3-21), we obtain an equation for the rate of change of temperature that does not explicitly depend on the rate of change of pressure of the system, i.e.

$$mc_p\dot{T} = \left(\sum_j \dot{m}_j h_j - \dot{Q}_w\right) - mc_\phi\dot{\phi} - h\dot{m} + mB\left(-\frac{\dot{V}}{V} - \frac{1}{\rho}\frac{\partial \rho}{\partial T}\dot{T} - \frac{1}{\rho}\frac{\partial \rho}{\partial \phi}\dot{\phi} + \frac{\dot{m}}{m}\right) \tag{3-23}$$

where $$B = \frac{1}{(\partial \rho / \partial p)}(1 - \rho c_T) \tag{3-24}$$

Dividing (3-23) by m, and collecting terms in $\dot{T}$, $\dot{\phi}$ and $\dot{m}$, we get

$$(c_p + \frac{B}{\rho}\frac{\partial \rho}{\partial T})\dot{T} = \frac{1}{m}(\sum_j \dot{m}_j h_j - \dot{Q}_w) - (c_\phi + \frac{B}{\rho}\frac{\partial \rho}{\partial \phi})\dot{\phi} + B\frac{\dot{m}}{m}(1 - \frac{h}{B}) - B\frac{\dot{V}}{V} \qquad (3\text{-}25)$$

leading to

$$\dot{T} = \frac{B}{A}[\frac{\dot{m}}{m}(1 - \frac{h}{B}) - \frac{\dot{V}}{V} - \frac{C}{B}\dot{\phi} + \frac{1}{Bm}(\sum_j \dot{m}_j h_j - \dot{Q}_w)] \qquad (3\text{-}26)$$

where

$$A = c_p + \frac{B}{\rho}\frac{\partial \rho}{\partial T} = c_p + \frac{(\partial \rho/\partial T)}{(\partial \rho/\partial p)}(\frac{1}{\rho} - c_T) \qquad (3\text{-}27)$$

$$C = c_\phi + \frac{B}{\rho}\frac{\partial \rho}{\partial \phi} = c_\phi + \frac{(\partial \rho/\partial \phi)}{(\partial \rho/\partial p)}(\frac{1}{\rho} - c_T) \qquad (3\text{-}28)$$

3.3 Application of Conservation Equations to Reciprocator Cycle

The above conservation equations can be applied to the thermodynamic processes of the four-stroke diesel cycle as follows:

i) Intake

$$\dot{m} = \dot{m}_{in} - \dot{m}_{ex} \qquad (3\text{-}29)$$

$$\dot{F} = \frac{\dot{m}_{in}}{m}(F_{in} - F) - \frac{\dot{m}_{ex}}{m}(F_{ex} - F) \qquad (3\text{-}30)$$

$$\dot{T} = \frac{B}{A}[\frac{\dot{m}}{m}(1 - \frac{h}{B}) - \frac{\dot{V}}{V} - \frac{C}{B}\dot{\phi} + \frac{1}{Bm}(\dot{m}_{in}h_{in} - \dot{m}_{ex}h_{ex} - \dot{Q}_w)] \qquad (3\text{-}31)$$

ii) Compression

$$\dot{m} = 0 \qquad (3\text{-}32)$$

$$\dot{F} = 0 \qquad (3\text{-}33)$$

$$\dot{T} = \frac{B}{A}\left[-\frac{\dot{V}}{V} - \frac{\dot{Q}_w}{Bm}\right] \qquad (3\text{-}34,$$

(iii) Combustion

$$\dot{m} = \dot{m}_f \qquad (3\text{-}35)$$

$$\dot{F} = \frac{\dot{m}_f}{m}(1 - F) \qquad (3\text{-}36)$$

$$\dot{T} = \frac{B}{A}\left[\frac{\dot{m}_f}{m}\left(1 - \frac{h}{b}\right) - \frac{\dot{V}}{V} - \frac{C}{B}\dot{\phi} + \frac{1}{BM}(\dot{m}_f h_f - \dot{Q}_w)\right] \qquad (3\text{-}37)$$

where h_f is the absolute fuel enthalpy, given by (B-1).

(iv) Exhaust

$$\dot{m} = -\dot{m}_{ex} \qquad (3\text{-}38)$$

$$\dot{F} = -\frac{\dot{m}_{ex}}{m}(F_{ex} - F) \qquad (3\text{-}39)$$

$$\dot{T} = \frac{B}{A}\left[-\frac{\dot{m}_{ex}}{m}\left(1 - \frac{h}{B}\right) - \frac{\dot{V}}{V} - \frac{C}{B}\dot{\phi} + \frac{1}{Bm}(-\dot{m}_{ex} h_{ex} - \dot{Q}_w)\right] \qquad (3\text{-}40)$$

Note that the fuel fraction of the mass flow rate through the exhaust port, F_{ex}, could be different from the cylinder fuel fraction, F, in reverse flow situations.

4. MODELING OF RECIPROCATOR ENGINE PROCESSES

4.1 Gas Exchange

A one-dimensional quasi-steady compressible flow model is used to calculate the mass flow rates through the intake and the exhaust valves during the gas exchange process. The intake manifold and the exhaust port are treated as plenums with known pressures. Furthermore, the temperature and average equivalence ratio of the intake charge (fresh air at intake manifold conditions) and the exhaust charge (mixture of air and combustion products at cylinder conditions) are known. When reverse flow into the intake manifold occurs, a rapid-mixing model is used, i.e., instantaneous mixing between the back-flowing charge and the intake charge is assumed.

At each step of the gas exchange process, values for the valve open areas and discharge coefficients are obtained from tabulated data. Given the open area, the discharge coefficient, and the pressure ratio across a particular valve, the mass flow rate across that valve is calculated from:

$$\dot{m} = c_d A \frac{p_o}{RT_o}\sqrt{\gamma RT_o}\left\{\frac{2}{\gamma-1}\left[\left(\frac{p_s}{p_o}\right)^{2/\gamma} - \left(\frac{p_s}{p_o}\right)^{(\gamma+1)/\gamma}\right]\right\}^{1/2} \qquad (4\text{-}1)$$

where

c_d = discharge coefficient

A = valve open area

p_o = stagnation pressure upstream of restriction

p_s = static pressure at restriction

T_o = stagnation temperature upstream of restriction

γ = ratio of specific heats

R = gas constant

When the kinetic energy in the cylinder is negligible, the stagnation pressure and temperature reduce to the static pressure and temperature, respectively. For the case of choked flow, equation (4-1) reduces to

$$\dot{m} = c_d A \frac{p_o}{RT_o} \sqrt{\gamma R T_o} \left(\frac{2}{\gamma+1}\right)^{(\gamma+1)/2(\gamma-1)} \qquad (4\text{-}2)$$

The mass, m(t), in the cylinder at any time t can be found from integration of the mass conservation equation (3-1), i.e.

$$m(t) = m_o + \int_{t_o}^{t} \dot{m}_{in}\,dt - \int_{t_o}^{t} \dot{m}_{ex}\,dt \qquad (4\text{-}3)$$

where m_o is the mass in the cylinder at the start of the cycle calculation, inlet valve opening (IVO).

4.2 Combustion Model

The diesel combustion process is a complex, unsteady, heterogeneous, three-dimensional process. A complete mathematical combustion analysis would require accurate models of compressible viscous air motion, fuel spray penetration, droplet break-up and evaporation, air entrainment into the spray, combustion kinetics, turbulent diffusion and so on. The details of the combustion process would depend on the characteristics of the fuel, the design of the combustion chamber and the fuel injection system, and on the engine's operating conditions. Although an adequate conceptual understanding of diesel combustion has been developed to date, a comprehensive quantitative model of all the individual processes has yet to be proposed.

A useful approach to the problem of combustion simulation has been to model combustion as a heat release process, as originally proposed by Lyn [7]. The rate of heat release (or, equivalently, the rate of fuel burning) can be defined as the rate at which the chemical energy of the fuel is released by

combustion. Based on heat release analysis and high-speed photography, Lyn has provided an excellent description of the different stages of diesel combustion. These stages can be identified on the typical rate of heat release diagram for a DI engine shown in Fig. 2 as follows:

Ignition delay: The period between the start of injection (the point at which the injector needle starts to lift) and ignition (the start of positive heat release due to combustion).

Pre-mixed or rapid combustion phase: In this phase, combustion of the fuel which has mixed with air to within the flamability limits during the ignition delay period occurs rapidly in a few crank angle degrees. This results in the high initial rate of burning generally observed in direct-injection diesel engines.

Mixing controlled combustion phase: Once the fuel and air premixed during the ignition delay have been consumed, the heat release rate (or burning rate) is controlled by the rate at which mixture becomes available for burning. The heat release rate may or may not reach a second (usually lower) peak in this phase; it decreases as this phase progresses.

Late combustion phase: Heat release continues at a low rate well into the expansion stroke. Eventually, the burning rate asyptotically approaches zero. The nature of combustion during this phase is not well understood. Possible processes are that a small fraction of the fuel may not yet have burned, or energy present in soot and fuel-rich combustion products can still be released, etc. Given the somewhat arbitrary limits of this phase, combustion models usually focus on the main heat release periods, i.e. the pre-mixed and mixing controlled combustion phases.

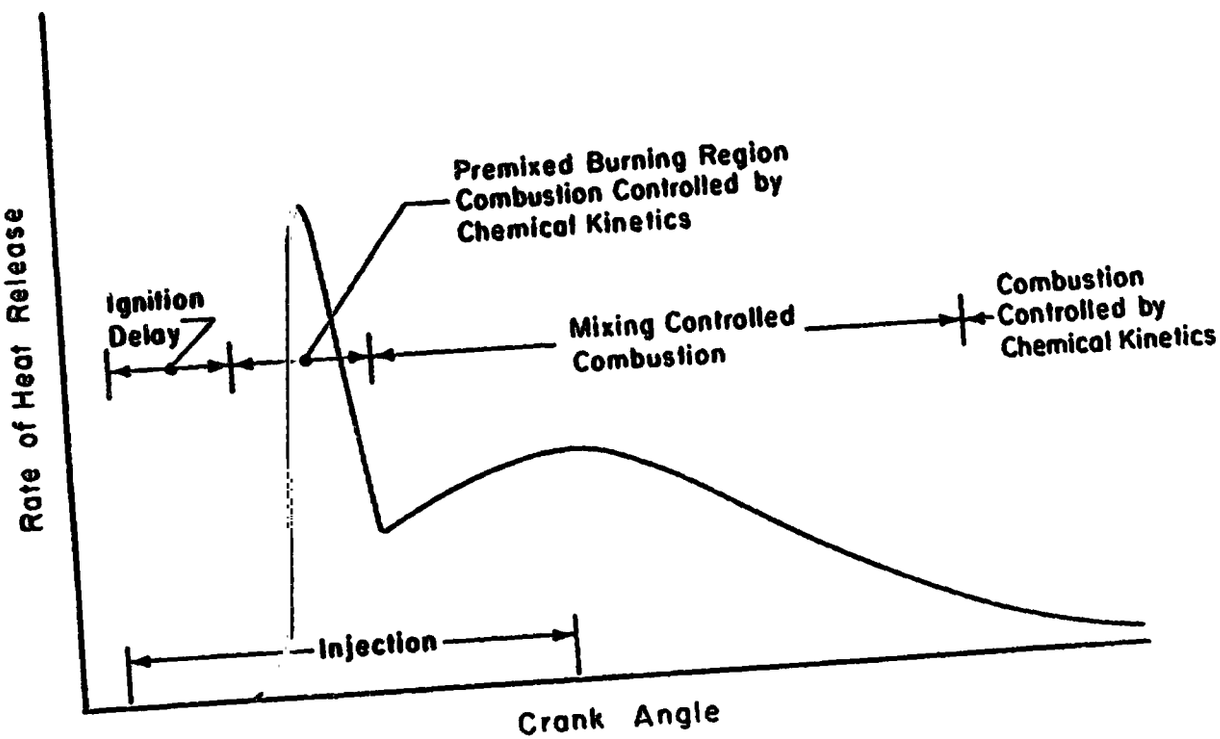

Fig. 2: Typical rate of heat release diagram for a direct-injection diesel engine.

Based on his observations, Lyn [7] proposed a method of predicting burning rates from tne rate of fuel injection. The fuel injected is divided into elements according to the order in which they enter the combustion chamber. These fuel elements become "ready for burning" according to a certain law. Thus, a "ready for burning" diagram can be obtained from the rate of injection diagram. At the ignition point, which occurs after the lapse of the delay period, the part of the injected fuel which has already been made "ready for burning" is added onto the current "ready for burning" diagram, causing the initial sharp peak in the burning rate diagram. Subsequent burning is essentially governed by the rate of injection. Although this method gives a reasonable fit to data obtained over a wide range of speeds and loads, it requires further refinement and calibration before it can be used in computer simulation work.

An alternative approach to modelling combustion, in the context of computer simulations predicting engine performance, is to describe the apparent fuel burning rate by algebraic expressions. The constants in these expressions can be chosen suitably to reflect the dependence of the actual fuel burning rate on engine type and particular operating conditions.

Shipinski et al [8] attempted to correlate the apparent rate of fuel burning with the rate of fuel injection by fitting a Wiebe function to heat release diagrams obtained from tests on a high-speed swirl-type direct injection engine. Although Shipinski obtained a reasonable agreement with his engine data, the heat release shape defined by the Wiebe function alone has a notable difference from the two-part characteristic with the initial spike that is measured on most engine types.

To overcome this problem, Watson et al [9] proposed that the apparent fuel burning rate could be expressed as the sum of two components, one relating to pre-mixed and the other to diffusion-controlled burning, i.e.

$$\dot{m}_t = \dot{m}_p + \dot{m}_d \tag{4-4}$$

where $\dot{m}$ is the fuel burning rate with respect to crank angle and subscripts t, p, d denote total, pre-mixed and diffusion burning, respectively.

In order to quantify the proportion of the fuel burnt by either mechanism, a phase proportionality factor, β, is introduced. This expresses the cumulative fuel burnt by pre-mixed burning as a fraction of the total fuel injected, i.e.

$$\beta = \frac{m_p}{m_t} \tag{4-5}$$

Consequently, a non-dimensional apparent fuel burning rate curve can be written as

$$\dot{M}_t(\tau) = \beta \dot{M}_p(\tau) + (1 - \beta)\dot{M}_d(\tau) \tag{4-6}$$

where $\dot{M}(\tau)$ is the non-dimensional burning rate distribution, and τ the normalized crank position.

The phase proportionality factor, β, is considered to be controlled by the length of the ignition delay period (since the fuel that is prepared for burning during this period governs the pre-mixed burning phase), and the overall cylinder equivalence ratio, ϕ_{ove}. This can be expressed by a relation of the form

$$\beta = 1 - a\frac{\phi_{ove}^{\ b}}{ID^c} \tag{4-7}$$

where ID is the ignition delay (see Section 4.3), and a, b, c are suitable constants to fit engine cylinder pressure data.

Futhermore, Watson concluded that the best representation of the experimental data was achieved using the following exponent burning rate distributions:

Premixed burning:

$$M_p(\tau) = 1 - (1 - \tau^{C_{p1}})^{C_{p2}} \qquad (4\text{-}8a)$$

or

$$\dot{M}_p(\tau) = C_{p1}C_{p2}\tau^{(C_{p1}-1)}(1 - \tau^{C_{p1}})^{(C_{p2}-1)} \qquad (4\text{-}8b)$$

Diffusion controlled burning (Wiebe function)

$$M_d(\tau) = 1 - \exp(-C_{d1}\tau^{C_{d2}}) \qquad (4\text{-}9a)$$

or

$$\dot{M}_d(\tau) = C_{d1}C_{d2}\tau^{(C_{d2}-1)}\exp(-C_{d1}\tau^{C_{d2}}) \qquad (4\text{-}9b)$$

where C_{p1}, C_{p2}, C_{d1}, C_{d2} are shape factors. The shape factors in equations (4-8) and (4-9) can be determined as a function of the engine operating conditions.

Using data from three typical turbocharged truck engines, (design details are summarized in Table 1), Watson established that the pre-mixed burning factors C_{p1} and C_{p2} were adequately modeled, for all three designs , by the following correlations:

$$C_{p1} = 2.0 + 1.25 \times 10^{-8}(ID \times N)^{2.4} \qquad (4\text{-}10a)$$

$$C_{p2} = 5000 \qquad (4\text{-}10b)$$

where ID = ignition delay, ms (see Section 4.3)

N = engine speed, RPM

TABLE 1

Appropriate Heat Release Profile Constants
For Different Engine Designs

ENGINE	A	B	C
a	0.296	0.95	0.81
b	0.37	0.41	0.28
c	0.26	0.28	0.51
k_1	14.2	16.67	7.54
k_2	0.644	0.6	0.65
k_3	0.79	1.2	0.93
k_4	0.25	0.13	0.22

Engine A: 6-cylinder, in-line, turbocharged, 4 stroke, DI, with inlet port swirl generation, and deep bowl combustion chamber.

Engine B: V8, turbocharged and intercooled, DI, 4 stroke, diesel engine.

Engine C: Turbocharged and intercooled, but more highly rated than engine A or B.

Source: Ref. [10]

The difusion burning factors C_{d1}, controlling the rate and duration of diffusion burning, and C_{d2}, controlling the timing of the peak diffusion burning rate, were modeled by correlations of the form

$$C_{d1} = k_1 \, \phi_{ove}^{-k_2} \tag{4-11a}$$

$$C_{d2} = k_3 \, C_{d1}^{k_4} \tag{4-11b}$$

where ϕ_{ove} is the overall cylinder equivalence ratio, and k_1, k_2, k_3, k_4 are constants appropriate for each combustion chamber design. Table 1 summarizes the values for the diffusion-burning constants in equation (4-11) and the phase-proportonality constants in equation (4-7) that Watson etablished for the three engines used in his tests.

In our engine simulation, we have followed Watson's approacn to describe the heat release profile. As a starting point, Watson's constants for Engine A were used to describe our engine. However, at full load and rated speed conditions, the calculated peak cylinder pressure and the brake mean effective pressure were correspondingly found to be 26% and 6.6% higher than test data obtained at Cummins. In order to calibrate these constants for our engine design, an iterative procedure was followed [10], where the shape factors C_{d1} and C_{d2} were modified until the calculated cylinder pressure diagram was in good agreement with the pressure data that we obtained from Cummins (one pressure trace, at rated load and speed, at a given injection timing).

We concluded that the Engine A values for a, b, c, k_1, k_2 and k_4 were adequate, while k_3 would have to be close to 1.05. These values were used in all our subsequent calculations.

4.3 Ignition Delay Model

The ignition delay period in a diesel engine was defined in section 4.2 as the time (or crank angle) interval between the start of injection and the start of combustion. The start of injection is usually taken as the time when the injector needle lifts off its seat (determined from a needle lift indicator). The start of combustion is more difficult to determine. It is best identified from the change in slope of the heat release rate versus time curve which occurs at ignition.

Both physical and chemical processes must take place before the injected fuel can burn. The physical processes are: the atomization of the liquid fuel jet; the vaporization of the fuel droplets; the mixing of fuel vapor with air. The chemical processes are the precombustion reactions of the fuel, air, residual-gas mixture which lead to autoignition. These processes are affected by engine design and operating variables, and fuel characteristics.

Ignition delay data from fundamental experiments in combustion bombs and flow reactors have usually been correlated by equations of the form

$$ID = A\, p^{-n} \exp(E/RT) \qquad (4\text{-}12)$$

where ID = ignition delay, ms

E = apparent activation energy for the fuel autoignition process

R = universal gas constant

p = gas pressure, atm

T = gas temperature, Kelvins

and A and n are constants dependent on the fuel and the injection and air-flow characteristics. Representative values for A, n and E are given in Table 2. Additional details can be found in [11]-[13].

TABLE 2

Constants for Arrhenius Equation
for Ignition Delay [ms]

Fuel	A	n	E/R Kelvins	Ref.
diesel	3.45	1.02	2100	[9]
diesel	53.5	1.23	676.5	[11]
n-cetane	0.872	1.24	4050	[11]
n-heptane	0.748	1.44	5270	[11]
diesel	4.05×10^{-2}	0.757	5470	[12]
diesel	2.43×10^{-6}	2	20915.3	[13]
kerosene	1.68×10^{-5}	2	19008.7	[13]
cetane	4.04×10^{-10}	2	25383	[13]

These correlations have usually been derived from tests in uniform air environments where the pressure and temperature only changed due to the cooling effect of the fuel vaporization and fuel heating processes. However, in a diesel engine, pressure and temperature change considerably during the delay period due to the compression resulting from piston motion. Another problem is that the form of these simple correlations is not sufficiently flexible to allow all the influencing fuel and engine parameters to be included in the calculation of the ignition delay.

Hardenberg and Hase [14] have developed an empirical formula for predicting the ignition delay in DI engines as a function of fuel characteristics, engine parameters and ambient conditions. Dent [15] has shown that this formula can give reasonable agreement with experimental data over a wide range of engine conditions. However, the pressure and temperature used in this correlation are identified as the corresponding conditions at top deal centre, estimated using a polytropic model for the compression process. It is felt that such a polytropic model is not appropriate in our simulation context, where pressures and temperatures can be accurately predicted over the duration of the ignition delay period.

We have included two approaches for ignition delay in this simulation:

a. The crank angle at start of combustion can be specified: this often is useful when it is desired to suppress changes in combustion timing (which may shift the combustion process relative to its optimum location in the cycle).

b. The ignition delay period is calculated as the difference between the time at which combustion occurs (t_{ign}) and the time at which injection starts (t_{inj}). The time t_{ign} is obtained by integrating over the duration of the ignition delay period the reciprocal of the predicted

ignition delay at each time step until the following relationship is satisfied:

$$\int_{t_{inj}}^{t_{ign}} \frac{dt}{ID(t)} = 1 \qquad (4\text{-}13)$$

where the instantaneous estimates of the ignition delay are calculated from an equation of the form of (4-12), with pressure and temperature taken at their instantaneous values.

4.4 Heat Transfer

The heat transfer mechanisms in a diesel engine include forced convection ($\dot{Q}_c$) from the turbulent flow in the cylinder to the combustion chamber walls, and radiation ($\dot{Q}_r$) from the flame and the burning soot particles. The total heat transfer rate ($\dot{Q}_w$) is therefore given by

$$\dot{Q}_w = \dot{Q}_c + \dot{Q}_r \qquad (4\text{-}14)$$

4.4.1 Convective heat transfer

The convective heat transfer at the gas-to-cylinder wall interface will depend on the temperature gradient in the boundary layer at the surface. However, due to the inherent difficulties in calculating the details of turbulent fluid motion in the combustion chamber during the operating cycle of the engine, the convective heat transfer rate is usually expressed as

$$\dot{Q}_c = h\,A\,(T_g - T_w) \qquad (4\text{-}15)$$

where

h = convective heat transfer coefficient

A = surface area

T_g = bulk mean gas temperature

T_w = inside wall surface temperature of cylinder head, piston, or liner, as appropriate.

The problem is then to devise a method to calculate the convective heat transfer coefficient that appears in (4-15). The approach usually taken is to calculate h from a Nusselt-Reynolds number correlation analogous to that used for steady turbulent flow in a pipe [16]-[20], i.e.,

$$Nu = a\, Re^d\, Pr^e \tag{4-16}$$

where

$Nu = hL/\lambda$: Nusselt number

$Re = VL/\nu$: Reynolds number

$Pr = \mu c_p/\lambda$: Prandtl number

L = a characteristic length

V = a characteristic velocity

λ = thermal conductivity

ν = kinematic viscosity

μ = dynamic viscosity

ρ = density

c_p = specific heat at constant pressure

and a, d, e are constants adjusted to fit experimental data.

Fortunately, there is little variation in the Prandtl number for air and combustion products, which is usually close to unity. Consequently, we may drop the Prandtl number dependence in equation (4-16) with little loss in accuracy, so that

$$Nu = a\, Re^d \tag{4-17}$$

To calculate the convective heat transfer coefficient from correlation (4-17), instantaneous values for the characteristic length and velocity scales, and the gas transport properties (μ, ρ, and λ) are needed. Currently, it is not possible to predict these parameters and their spatial and temporal variation with any accuracy in an internal combustion engine. To overcome this difficulty, representative values of the characteristic length and velocity scales, and the gas temperature, pressure, and equivalence ratio at which the gas properties are to be evaluated are chosen.

For our heat transfer model, the characteristic length scale is taken to be the macroscale of turbulence, as defined by equation (4-36). The characteristic velocity V is postulated to be an effective velocity due to contributions from the mean kinetic energy, the turbulent kinetic energy and piston motion, i.e.

$$V = [U^2 + u'^2 + (V_p/2)^2]^{1/2} \qquad (4\text{-}18)$$

where

U = mean flow velocity, defined by (4-28)

u' = turbulent intensity, defined by (4-29)

V_p = instantaneous piston speed

While this expression for V is speculative, it is constructed in such a way that increases in any of the three component velocities lead to increases in the heat transfer rate, while at the same time errors due to overestimating the contribution from any one component are minimized.

Many attempts have been reported to determine the constants a and d, through curve-fitting experimental results [16]-[20]. Suggested values are

$$a = 0.035 \text{ to } 0.13$$
$$d = 0.7 \text{ to } 0.8 \qquad (4\text{-}19)$$

depending on intensity of change motion. The gas density and the transport properties, μ and λ, that appear in correlation (4-17) are evaluated at the mean gas temperature, pressure, and equivalence ratio of the cylinder contents (see Appendix C).

4.4.2 Radiative heat transfer

The primary sources of radiative heat transfer in a diesel engine are the high temperature burned gases and the soot particles which are formed as an intermediate step in the turbulent diffusion-controlled diesel flame. Because the particle size distribution, number density, and temperature, and flame geometry are not well defined in a diesel engine, direct measurements of radiation on operating engines are required.

Estimates of the relative importance of radiation in cooled diesel engines have varied between a few and 50 percent of the total heat transfer [17],[18],[21]-[28]. The limited experimental engine radiation measurements to date are summarized in Table 3. In general, the radiant heat flux depends on the location on the combustion chamber surface, crank angle in the operating cycle, engine load, engine size, and engine design. At high load, the measurements suggest that the radiant heat flux is betwseen 25 and 45 percent of the total heat flux.

Due to the complexity of the problem, accepted prediction formulas for radiant heat flux in a diesel engine are not available. Annand [17] has proposed a radiation term based on the average bulk gas temperature of the form:

$$\dot{Q}_r = k_r A(T_g^4 - T_w^4) \qquad (4\text{-}20)$$

where k_r = empirical radiation constant

A = surface area

TABLE 3

Relative Importance of Radiant Heat Flux

Engine	Load Range	$\dot{Q}_r/\dot{Q}_w$ Peak Values	$\dot{Q}_r/\dot{Q}_w$ Mean Values	Ref.
DI, 4 stroke	Mid-Full	9-15	10-30	[21]
DI, 2 stroke	Full		35-45	[23]
Prechamber	Idle-Full		7-23	[24]
DI, swirl	Light-Full		0-40	[25]
DI, swirl 4 stroke	80%-Full	12-18		[26]
DI, swirl 4 stroke	Light-Full	70-13	21-14	[27] [28]

T_g = average bulk gas temperature

T_w = inside wall surface temperature of cylinder head, piston or liner, as appropriate.

During the intake, compression and exhaust processes, the radiative heat flux is taken to be zero. During combustion, Annand and Ma [18] suggested that

$$k_r = C_r \sigma \tag{4-21}$$

where σ is the Stephan-Boltzmann constant (56.7×10^{-12} kW/m^{2}K^4), and C_r is an adjustable calibrating constant with values in the range of 0.6-3.1, depending on the engine speed and load. Note that since the temperature used is the average bulk temperature and not the flame temperature, C_r is not an emissivity. Limited evaluation of this approach has shown that $C_r = 0.6$ gave approximately correct radiant flux magnitude for one engine but was too low for another [21], while $C_r = 1.6$ gave radiant heat fluxes higher than experimental data [22]. Flynn et al [28] have measured the instantaneous radiant heat transfer in a direct-injection diesel engine under a wide range of engine operating conditions. A monochromator was used to measure intensity of radiation at seven wavelengths. By assuming a monochromatic emissivity law consistent with observed radiation from very small particles [29] and integrating over all wavelenghts, Flynn et al. obtained an apparent radiant temperature, an apparent grey-body emissivity, and a total radiant heat transfer rate at each crank angle during the cycle. The results of Flynn's work indicate that the apparent radiant temperature is much higher than the average bulk gas temperature. In fact, during the time of peak heat release, the apparent radiant temperature was found to be very close to the flame temperature. Furthermore, during the period of maximum radiation, the apparent emissivity was 0.8 to 0.9, and it dropped almost linearly to zero by the end of the combustion process.

In the light of Flynn's results, and due to the absence of any real fundamental basis or experimental support for Annand's model, an alternative radiation model was developed for the present work. The instantaneous radiant heat flux is expressed as

$$\dot{Q}_r = \varepsilon_a \sigma A (T_r^4 - T_w^4) \qquad (4\text{-}22)$$

where ε_a = apparent grey-body emissivity

σ = Stephan-Boltzmann constant

A = surface area

T_r = apparent radiant temperature

Flynn's data suggest that the apparent radiant temperature is close to the adiabatic flame temperature during the period of peak heat release. The adiabatic flame temperature can be modeled as the temperature of slightly greater than stoichiometric zones of hydrocarbon-air combustion products, i.e., $T(\phi = 1.1)$. However, as combustion progresses and relatively fewer close-to-stoichiometric fuel-air zones are found in the cylinder, this adiabatic flame temperature becomes considerably higher than Flynn's apparent radiant temperature [28]. A better estimate (in reasonable agreement with the data) of the apparent radiant temperature was found to be the mean of the adiabatic flame temperature and the average bulk gas temperature, i.e.

$$T_r = \frac{T_g + T(\phi = 1.1)}{2} \qquad (4\text{-}23)$$

The temperature of combustion products at an equivalence ratio of 1.1, $T(\phi = 1.1)$, is computed as a function of the instantaneous air temperature and pressure from a correlation obtained by applying a least-squares curve-fitting technique to results of the NASA equilibrium program [30], for constant pressure hydrocarbon-air combustion. Satisfactory accuracy (less than 1% error) was obtained by considering two adjacent air temperature ranges, i.e.:

$$T(\phi = 1.1) = [1 + 0.0002317(T_{air} - 950)] \times (2726.3 + 0.9306p - 0.003233p^2)$$

$$\text{for } 800\ K < T_{air} < 1200\ K \qquad (4\text{-}24)$$

$$T(\phi = 1.1) = [1 + 0.000249\ (T_{air} - 650)] \times (2497.3 + 4.7521p - 0.11065p^2 + 0.000898p^3)$$

$$\text{for } 450\ K < T_{air} < 800\ K. \qquad (4\text{-}25)$$

The instantaneous air temperature, T_{air}, is calculated assuming adiabatic compression of the air from the condition at the start of combustion (subscript ign), i.e.

$$T_{air} = T_{air,ign}(p/p_{ign})^{(\gamma-1)/\gamma} \qquad (4\text{-}26)$$

where γ is the ratio of specific heats for air at the instantaneous temperature and pressure.

The apparent emissivity is assumed to vary linearly between its maximum value (taken as 0.9) and zero over the duration of the combustion process, i.e.

$$\epsilon_a(t) = 0.9\left(1 - \frac{t - t_{ign}}{t - t_{evo}}\right) \qquad (4\text{-}27)$$

where t_{evo} is the time when the exhaust valve opens.

4.5 Turbulent Flow Model

The heat transfer model of the cycle simulation requires estimates of the characteristic velocity and length scales. To estimate these scales in a way which incorporates the key physical mechanisms affecting charge motion in the cylinder, a turbulent flow model is used. This model is a variation of the

models used by Mansouri et al [31], Poulos and Heywood [32] in previous engine simulation work.

The turbulence model consists of a zero-dimensional energy cascade. Mean flow kinetic energy, K, is supplied to the cylinder through the valves. Mean kinetic energy, K is converted to turbulent kinetic energy, k, through a turbulent dissipation process. Turbulent kinetic energy is converted to heat through viscous dissipation. When mass flows out of the cylinder, it carries with it both mean and turbulent kinetic energy. Figure 3 illustrates the energy cascade model.

At any time during the cycle, the mean flow velocity, U, and the turbulent intensity, u', are found from knowledge of the mean and turbulent kinetic energies, K and k, respectively. Thus, the following equations apply:

$$K = \frac{1}{2} m U^2 \tag{4-28}$$

$$k = \frac{3}{2} m u'^2 \tag{4-29}$$

where the factor 3 in equation (4-29) comes from assuming that the small scale turbulence is isotropic (and accounting for all three orthogonal fluctuating velocity components).

The time rate of change of the mean kinetic energy, K is given by

$$\frac{dK}{dt} = \frac{1}{2} \dot{m}_i V_i^2 - P - K \frac{\dot{m}_e}{m} \tag{4-30}$$

Similarly, the rate of change of the turbulent kinetic energy, k, is

$$\frac{dk}{dt} = P - m\varepsilon - k \frac{\dot{m}_e}{m} + A \tag{4-31}$$

with $$\varepsilon = \frac{u'^3}{\ell} = \frac{(2k/3m)^{3/2}}{\ell} \tag{4-32}$$

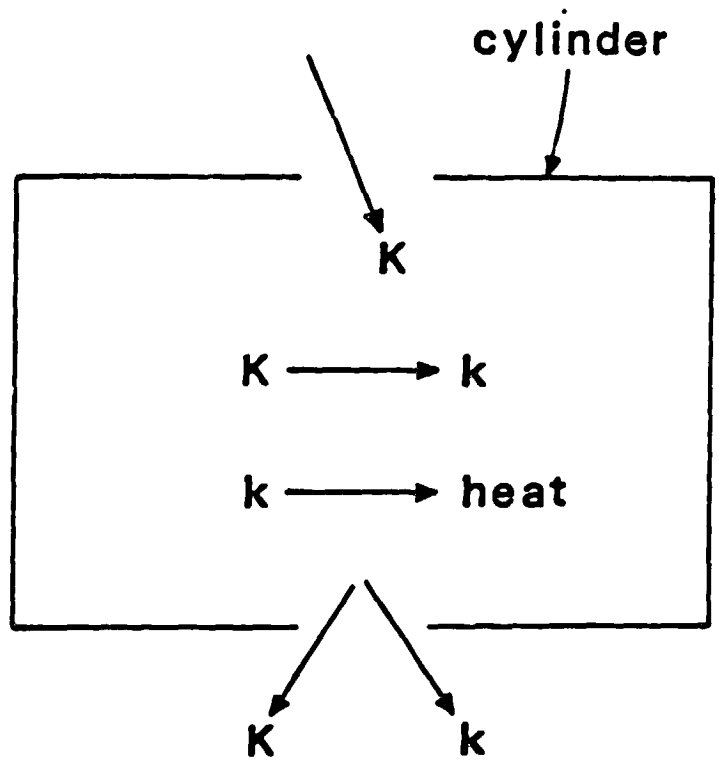

Fig. 3: Energy cascade model

where m = mass in the cylinder

$\dot{m}_i$ = mass flow rate into the cylinder

$\dot{m}_e$ = mass flow rate out of the cylinder

V_i = jet velocity into the cylinder

P = rate of turbulent kinetic energy production

ε = rate of turbulent kinetic energy dissipation per unit mass

A = rate of turbulent kinetic energy amplification due to rapid distortion

ℓ = characteristic size of large-scale eddies

In equations (4-30) and (4-31), the production term P has to be defined in terms of flow and geometrical parameters of the chamber. However, since the above model does not predict spatially resolved flow parameters, P must be estimated from mean flow quantities only.

Assuming that turbulence production in the engine cylinder is similar to turbulence production in a boundary layer over a flat plate [33], we can express P as

$$P = \mu_t \left(\frac{\partial U}{\partial y}\right)^2 \tag{4-33}$$

where $\mu_t = C_\mu k^2/(m\varepsilon)$ is turbulent viscosity, and $C_\mu = 0.09$ is a universal constant. Again, as the velocity field in the cylinder is not known, the velocity gradient $(\partial U/\partial y)$ is approximated as

$$\left(\frac{\partial U}{\partial y}\right)^2 = C_\beta \left(\frac{U}{L}\right)^2 \tag{4-34}$$

where C_β is an adjustable constant and L is a geometric length scale.

Using equations (4-33), (4-34), (4-28) and (4-32), we can express P as

$$P = 2\left(\frac{3}{2}\right)^{3/2} C_\mu C_\beta \left(\frac{K\ell}{L^2}\right)\left(\frac{k}{m}\right)^{1/2} \qquad (4\text{-}35)$$

Furthermore, the characteristic size of the large-scale eddies, ℓ, and the representative geometric length scale, L will be both identified with the macroscale of turbulence, assumed to be given by

$$\ell = L = V/(\pi B^2/4) \qquad (4\text{-}36a)$$

where V is the instantaneous volume of the combustion chamber and B is the cylinder bore, subject to the restriction that

$$L \leq B/2 \qquad (4\text{-}36b)$$

Hence, equation (4-35) can be re-written as

$$P = 0.3307\, C_\beta \left(\frac{K}{L}\right)\left(\frac{k}{m}\right)^{1/2} \qquad (4\text{-}37)$$

During the compression and the combustion processes, the turbulent kinetic energy decays due to viscous dissipation. At the same time the turbulent kinetic energy is amplified due to the rapid distortion that the cylinder charge undergoes with rising cylinder pressures. Consequently, an amplification term, A, was added to equation (4-31) to account for this effect. The amplification term will be larger during combustion when the unburned gas is assumed to be compressed by the flame at a sufficiently high rate. However, in the diesel engine context of high compression ratios, the amplification term is included during compression, too.

Using equation (4-29), the rate of turbulence amplification due to rapid distortion can be expressed as

$$A = 3\, m\, u' \frac{du'}{dt} \qquad (4\text{-}38)$$

where the rate of change of the turbulent intensity du'/dt can be estimated assuming that conservation of mass and angular momentum can be applied to the large scal eddies during the rapid distortion period.

Under these assumptions, conservation of mass for a single eddy of volume V_L requires that

$$\rho V_L = \rho_o V_{Lo} \tag{4-39}$$

where ρ is the mean gas density and subscript o refers to the conditions at the start of compression. Then, since

$$V_L \sim L^3 \tag{4-40}$$

where L is the macroscale of turbulence, we can re-write (4-39) as

$$\frac{L}{L_o} = \left(\frac{\rho_o}{\rho}\right)^{1/3} \tag{4-41}$$

Conservation of eddy angular momentum requires that

$$U_\omega L = U_{\omega o} L_o \tag{4-42}$$

where U_ω is the characteristic velocity due to eddy vorticity.

Combining (4-41) and (4-42) with the assumption that

$$U_\omega \sim u' \tag{4-43}$$

the following relation is obtained for the evolution of the turbulent intensity during the rapid compression period

$$\frac{u'}{u'_o} = \left(\frac{\rho}{\rho_o}\right)^{1/3} \tag{4-44}$$

Differentiating both sides of equation (4-44) and re-arranging we get

$$\frac{du'}{dt} = \frac{u'}{3\rho}\frac{d\rho}{dt} \tag{4-45}$$

Hence, combining equations (4-38) and (4-45), the rate of turbulence amplification is given by

$$A = \frac{mu'^2}{\rho}\frac{d\rho}{dt} \qquad (4\text{-}46)$$

or, introducing (4-29),

$$A = \frac{2}{3} k \frac{\dot{\rho}}{\rho} \qquad (4\text{-}47)$$

with $\dot{\rho}$ given from equation (3-15).

4.6 Engine Friction Model

To convert indicated engine performance quantities to brake engine performance quantities, engine friction estimates are required. However, the measurement and analysis of engine frictional losses are yet to be satisfactorily resolved. This is primarily due to the inherent problem of direct, accurate measurement of these losses under actual running conditions. This problem occurs because the total loss is a summation of losses arising from the operation of the many components of the engine, and these components respond differently to changes in pressure, temperature and speed.

Direct motoring of an engine is the common method of measuring losses, but clearly the motoring losses are not the same as the losses under firing conditions. Some of the reasons are the lower pressure acting on piston rings and bearings, the lower temperatures of the piston and cylinder bore surfaces and thus the greater oil viscosity, the greater running clearance of the piston, and the missing exhaust blowdown period.

Nevertheless, a breakdown analysis of motoring losses supplemented by experiments on piston and ring friction rigs can be used to identify the

relative importance of the many components of the total friction and their response to changes in design variables. In general, the components of the losses expressed in terms of mean effective pressure, mep, tend to fall into three groups:

(i) Losses due to boundary lubrication, where the friction forces are approximately invarient with speed. These losses are undoubtedly influenced by the compression ratio.

(ii) Losses associated with hydrodynamically lubricated surfaces in relative motion, which vary directly with speed. All major rotating parts fall into this group.

(iii) Losses associated with fluid (air, water and oil) pumping, which vary as the square of the speed.

Therefore, the motoring losses can be expressed in the form

$$F = A + BN + CN^2 \qquad (4\text{-}48)$$

where F are the losses in mep, N is engine speed, and A, B and C are constants.

Millington and Hartles [34] have measured motoring losses on a large variety of automotive diesel engines during the course of development of prototype engines. Their work suggests a readjustment of equation (4-48) coupled with suitable selection of the constants as follows:

$$F = A + 7.0 \frac{N}{1000} + 1.5 \left(\frac{V}{1000}\right)^2 \qquad (4\text{-}49)$$

where F = motoring mep, psi

A = compression ratio minus 4 for a DI diesel

N = engine speed, RPM

V = mean piston speed, ft/min

Equation (4-49) represents a sound empirical correlation of the motoring loss data obtained from diesel engines. It is used to obtain brake quantities from the indicated quantities computed in the engine simulation.

5. MODELING OF OTHER SYSTEM COMPONENTS

5.1 Turbomachinery Modeling

Steady-state performance maps give the interrelationships among mass flow rate, efficiency, pressure ratio and rotor speed for each of the three turbomachinery components: turbocharger compressor, turbocharger turbine and power turbine. The map variables of mass flow rate, $\dot{m}_{map}$, and rotor speed, ω_{map}, are corrected by factors relating actual inlet conditions to standard conditions. The speed correction factor involves inlet temperature, and the mass flow rate correction factor involves inlet temperature and pressure, so that

$$\omega_{map} = \omega_{actual}(T_{std}/T_{in})^{1/2} \tag{5-1}$$

$$\dot{m}_{map} = \dot{m}_{actual}(p_{std}/p_{in})(T_{in}/T_{std})^{1/2} \tag{5-2}$$

where the subscripts in and std refer to actual inlet and map standard inlet conditions, respectively.

The turbomachinery maps, usually obtained in graphical form, are entered into the simulation in tabular form, i.e. as a one-dimensional array of rotor speeds, ranked in ascending order; and a three-dimensional array of the remaining map variables, arranged as follows: for each of the speeds stored in the speed array, a uniform number of data points is recorded, each consisting of the values of mass flow, efficiency and pressure ratio at that point. The data points for each speed curve for each map are ranked in ascending order of pressure ratio. Note that for the compressor map this implies entering data in descending order of mass flow.

At a particular step in the cycle simulation, the tables need to be interpolated to find the necessary information. Appropriate routines were

developed to interpolate the performance maps of the various turbomachinery components. In general, these routines perform two-dimensional interpolation to calculate two unknown map variables from two known variables. Speed is always one of the two known variables and efficiency is one of the two unknown variables. Then, either mass flow rate is known and pressure ratio unknown, or vice-versa, depending on the turbomachinery component and the system configuration.

The method of map interpolation, as applied for example to the compressor map, is the following. Given a corrected speed, a search of the compressor speed array is performed, from the lowest value (i.e. the first array element) until a speed greater than the input speed is found. Using that greater speed and the speed just previous to that (the lesser speed), a speed interpolation parameter is calculated. This speed interpolation parameter is used to calculate values of pressure ratio at the input speed, until a pressure ratio greater than the input pressure ratio is found. This pressure ratio search, from low to high, will thus define a pressure ratio interpolation parameter. Then, using the speed and pressure ratio interpolation parameter, a two-dimensional linear interpolation is performed to calculate the mass flow and efficiency that correspond to the input values of speed and pressure ratio.

Certain important physical constraints must be considered in modeling turbomachinery component performance:

(a) Compressor Surge Line: When the mass flow rate through a compressor is reduced while maintaining a constant pressure ratio, a point arises at which local flow reversal occurs in the boundary layers. This will relieve the adverse pressure gradient until a new flow regime at a lower pressure ratio is established. Then, the flow will build up to the initial conditions, and thus flow instability will continue at a fixed

frequency. This phenomenon is called surge. Clearly, a compressor should not operate in the low-efficiency, unstable region, to the left of the surge line.

(b) Turbine Choking Characteristics: The mass flow range of a radial turbine, such as the turbocharger and the turbocompounded turbines, is limited by choking at high pressure ratios. The choking characteristics of the turbine are speed dependent. This effect is caused due to the centrifugal field created by the speed of the rotor.

To avoid any potential problems associated with the above constraints, certain provisions have been incorporated in the logic of the turbomachinery interpolation routines:

(i) Since the pressure ratio versus turbocharger speed line is fairly flat close to the compressor surge limit, small changes in pressure ratio can result in disproportionately large changes in output mass flow rate values. In order to avoid any oscillations in the system convergence procedure which could result in a substantial increase in computational time, the pressure ratio versus mass flow rate curves are modeled as single-valued, with a small, non-zero, slope close to the surge line.

(ii) During the turbocharger matching calculation, the rotor speed at some instant could become too low for the required boost pressure ratio. This means that the mass flow would have to be to the left of the surge boundary. Under these circumstances, the speed of the rotor is increased until an acceptable mass flow solution at the given input pressure ratio is obtained.

(iii) During the course of the simulation iterations, certain engine operating conditions could correspond to points that lie beyond the normal operating regime of the turbomachinery maps. Then, linear

extrapolation is performed to extend the range of the map characteristics. This extrapolation is subject to certain checks, so that the map regimes are not extended beyond the turbine choking characteristics or to the left of the compressor surge line. Furthermore, if the final converged solution for the engine-turbocharger matching is well beyond the normal map regimes, the turbomachinery used is not appropriate for the given engine design and operating conditions. The calculation should be repeated with more suitable turbomachinery components (different machine sizes, or higher component efficiencies).

5.2 Turbocharger Dynamics

The rate of change of the mechanical energy of the turbocharger rotor, $E_{t/c}$, depends on the difference between the power required to drive the compressor (negative), and the power delivered by the turbocharger turbine (positive):

$$\dot{E}_{t/c} = \dot{W}_{compressor} + \dot{W}_{turbine} \tag{5-3}$$

The change in mechanical energy relates to the change in rotor speed according to the turbocharger dynamics, i.e.,

$$\dot{E}_{t/c} = J\omega\dot{\omega} + B\omega^2 \tag{5-4}$$

where

J = rotational inertia of turbocharger

B = rotational damping of turbocharger

ω = angular velocity

The compressor and the turbine powers can be expressed as:

$$\dot{W}_{compressor} = \dot{m}_c(h_1 - h_2) \tag{5-5}$$

$$\dot{W}_{turbine} = \dot{m}_t(h_8 - h_9) \tag{5-6}$$

Solving for the change in speed $\dot{\omega}$ gives:

$$\dot{\omega} = \{(\dot{m}_c(h_1 - h_2) + \dot{m}_t(h_8 - h_9) - B\omega^2\}/J\omega \tag{5-7}$$

Note that the enthalpy changes across the compressor and turbine can be calculated assuming compressible flow across the two turbomachines, i.e.,

$$(h_1 - h_2) = -\frac{h_1}{\eta_c}\left[\left(\frac{p_2}{p_1}\right)^{R/c_p} - 1\right] \tag{5-8}$$

$$(h_8 - h_9) = \eta_t h_8\left[\left(\frac{p_8}{p_9}\right)^{R/c_p} - 1\right] \tag{5-9}$$

5.3 Turbocharger Matching Procedure

The simulation code is set up to analyze two different system configurations: i) a single-stage turbocharged diesel system and, ii) a turbocharged turbocompounded diesel system. Suitable turbocharger matching procedures have been developed for each case. These are summarized below.

5.3.1 Single-stage turbocharged case

The system configuration for this case is shown in Fig. 4. At a given instant, the values of the variables describing the state of the various system components are known (from the integration of the system governing equations over the previous time step). These include the intake and exhaust manifold pressures and the turbocharger rotor speed. Additionally, the

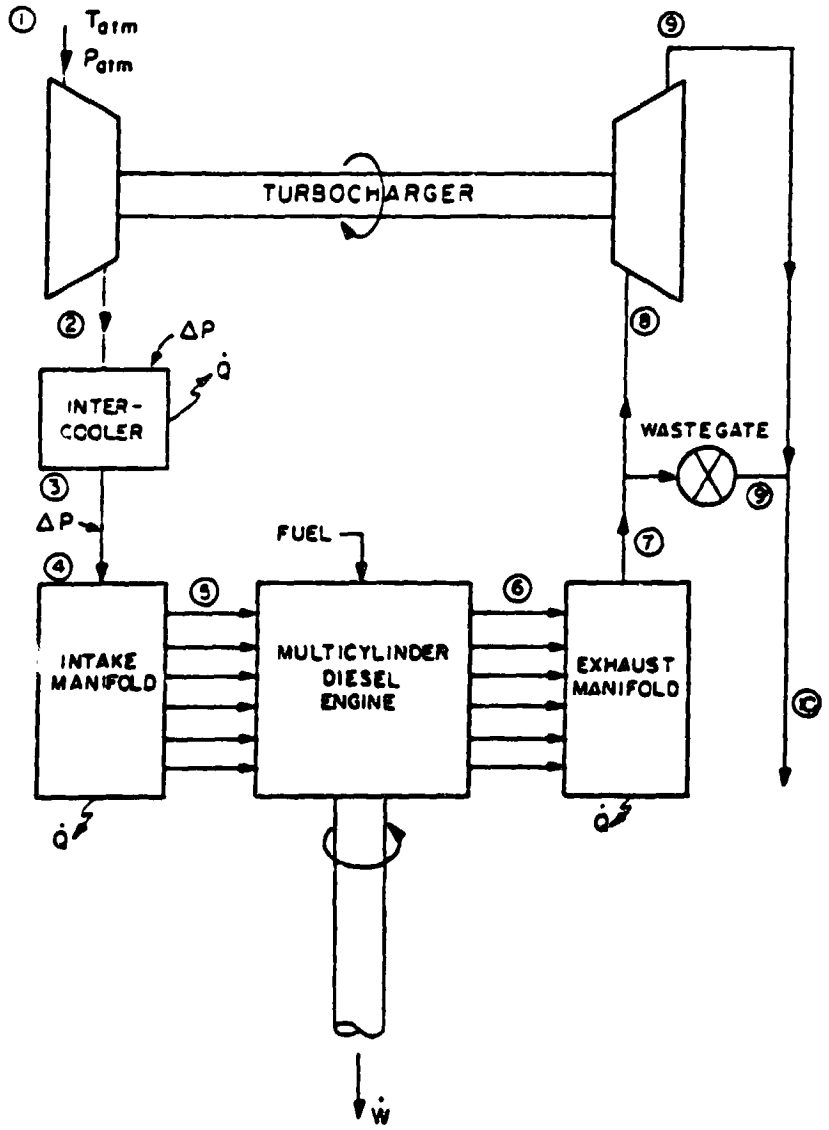

Fig. 4: Single-stage turbocharged system configuration.

compressor inlet pressure and the turbine exhaust pressure are fixed, i.e., atmospheric pressure less intake air filter pressure drop and atmospheric pressure plus muffler pressure drop, respectively. By relating the compressor discharge pressure to the intake manifold pressure and the turbine inlet pressure to the exhaust manifold pressure, through suitable pressure drops, the pressure ratio across each turbomachine is determined. Hence, the compressor and turbine maps can be entered using the calculated pressure ratios and the rotor speed (same for both turbomachines) as inputs. The output of the map interpolation routines determines the mass flow rate and efficiency for each component for the next time step. From these, the power required to drive the compressor, and the power delivered by the turbine are determined. Any excess power will result in a change in the rotor speed according to the turbocharger dynamics, i.e., Eq. (5-4). Finally, the values of the other state variables for the next time step will be determined from solution of the mass and energy conservation equations, where the compressor and turbine mass fluxes are taken from the output of the turbomachinery interpolation routines.

5.3.2 Turbocharged turbocompounded case

This case is relatively more complicated. For this system configuration, shown in Fig. 1, the intake side, and hence the compressor map treatment is identical to the single-stage turbocharged case. However, on the exhaust side, although the available pressure ratio can be defined as for the turbocharged case, the division of the pressure ratio between the two turbines is not known a priori. This calculation requires a special iterative procedure, based on continuity of mass flow through the exhaust system. At each time step, the calculation is started by assuming a mass flow going through the first turbine (taken as the value at the previous time step).

Then, the turbocharger turbine interpolation routine is entered with the mass flow rate and rotor speed as inputs. From the turbine pressure ratio returned by the routine, and the known exhaust manifold pressure, the first turbine exit pressure is determined. The latter, and the system exit pressure (atmospheric plus muffler pressure drop), specify the pressure ratio across the power turbine. Then, the power turbine map can be interpolated with the pressure ratio and shaft speed (gear ratio times reciprocator speed) as input, thus defining the mass flow through the power turbine. An updated estimate of the mass flow through the first turbine can be then calculated based on the previous estimate and the power turbine mass flow. The scheme used involves under-relaxation to increase the stability and efficiency of the matching procedure. For a converged solution, the mass flow through the turbocharger turbine (plus flow through the wastegate, if appropriate) must equal the flow through the power turbine. Once the turbocharger turbine flow and efficiency are established, the system state variables for the next time step can be determined following the same procedure as for the single-stage turbocharged case.

5.4 Intercooler Model

The intercooler, situated between the compressor discharge and the intake manifold, serves to increase the density of the charge air by lowering its temperature. The intercooler is modelled as a heat exchanger of fixed area, over-all heat-tranfer coefficient and cooling flow rate. The change in charge air temperature is determined from the non-dimensional heat exchanger effectiveness, ε,

$$\varepsilon = \frac{(T_{h1} - T_{h2})}{(T_{h1} - T_{c1})} \qquad (5\text{-}10)$$

where the subscripts h and c refer to the charge air flow (hot) and the coolant flow (cold) respectively; 1 and 2 refer to inlet and exit conditions; and

T_{h1} = compressor discharge temperature

T_{h2} = intercooler discharge temperature

T_{c1} = coolant inlet temperature (assumed to be fixed).

The heat exchanger effectiveness is either known as a design parameter, or can be derived from graphical correlations that are available for the various typical heat exchanger configurations [35]. From the latter, ε can be determined as a function of the capacity rate ratio, C_{min}/C_{max}, and the number of heat transfer units, N_A, where C_{min} and C_{max} are respectively the smaller and larger of the products of charge air and coolant flow rates with their respective specific heats, and

$$N_A = AU/C_{min}$$

where A = heat exchange surface area (fixed)

U = over-all heat transfer coefficient based on A.

Assuming that C_{max} is much larger than C_{min}, the expression for effectiveness reduces to the following simple form:

$$\varepsilon = 1 - \exp(-N_A) \qquad (5\text{-}11)$$

5.5 Exhaust Manifold Model

In most engine simulation programs of this type, the exhaust manifold is treated as a global open system [6]. A simple plenum is used with the exhaust gases from each cylinder flowing into the system and mixing with the all of the gases in the manifold. This approach has three primary disadvantages. First, the exhaust gases from a given cylinder are diluted by the gases in the

manifold in a manner that is not representative of a real manifold, where individual runners keep the gases from different cylinders separated during much of the flow path between the exhaust valve and the turbine. This dilution decreases substantially the gas temperature oscillations that occur in the manifold and at the turbine inlet.

The second disadvantage of a common plenum model is that it is not possible to follow the change in gas temperature as the gases flow through the exhaust manifold, mix with the gases in each section, and lose heat to the surroundings. With a common control volume, only one temperature is used to represent the temperature of the gases in the exhaust manifold. Again, this is not a good representation of a real exhaust manifold where the gas temperature varies along the length of the path between the exhaust valve and the turbine inlet.

The third disadvantage with a single control volume is that it is impossible to match the approximate volume, the inside surface area, and the cross-sectional area of a real manifold with only one set of dimensions for the model. The approximate volume is important for the accurate determination for the exhaust manifold pressure which in turn is an important factor in determining the turbocharger performance. The cross-sectional area and inside surface area are important for determining the temperature of the gases at the inlet to the turbocharger. With the single control volume approach, one is forced to compromise one or more of these geometric factors when specifying the dimensions of the manifold to be used for the simulation.

To avoid these disadvantages with a single plenum model, the exhaust manifold is divided into a series of connected open systems. The manifold is considered to be a composite of ports, runners, and a common plenum section. The port section is taken to be the volume contained within the head of the

engine. The runner represents the section of the manifold outside the head where the gases from one cylinder flow without mixing with the gases from any other cylinder. The plenum is defined as the volume where the gases from each of the engine cylinders, ports and runners are mixed before entering the turbine. A fourth system is also followed during the simulation that is composed of the runner from each cylinder and the plenum. This system has the properties that represent the average properties of the separate sub-systems, and it is used to determine the change in pressure in the manifold based on the overall mass balance.

As is done with the engine cylinders, the simulation only calculates the properties of the ports and runners for one master port and one representative master runner. The master port and runner information necessary to include the other cylinders in the engine calculation is stored in high-speed memory and is retrieved with the appropriate phase shift to determine what was occurring in other ports and runners at any given time during the cycle.

5.6 Manifold Conservation Equations

The general manifold open system model is shown in Fig. 5. The differential equations for the change in total mass and fuel fraction for the manifold come directly from the continuity relations derived earlier in Section 3.1, i.e.,

$$\dot{m}_m = \sum_j \dot{m}_j \,, \tag{5-12}$$

$$\dot{F}_m = \sum_j \frac{\dot{m}_j}{m_m} (F_j - F_m) \tag{5-13}$$

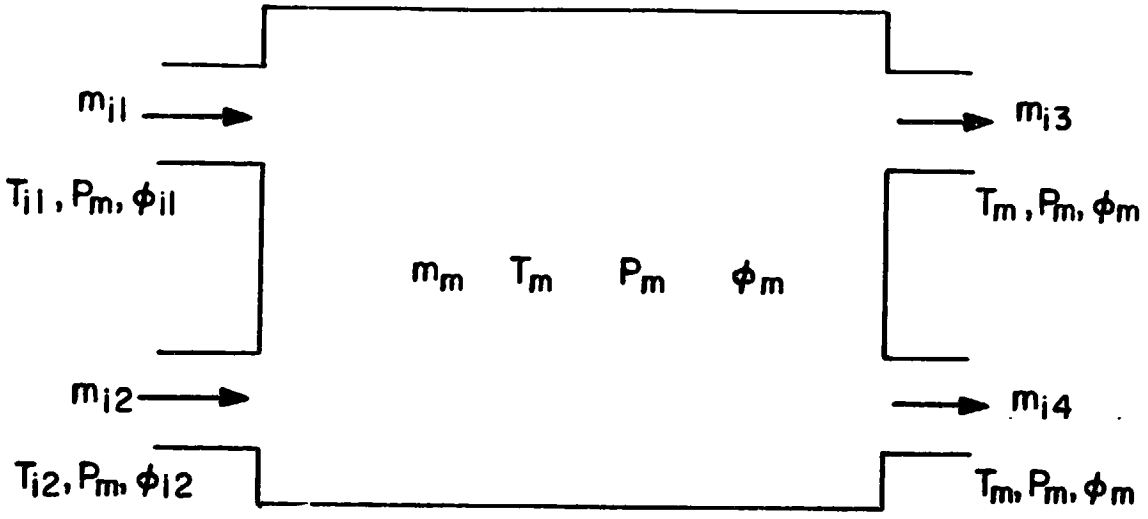

Fig. 5: General manifold open system.

where the subscript m refers to the intake manifold, or exhaust manifold section, and the subscript j refers to the j-th mass flow that enters or leaves the system of interest.

The mass flows entering and leaving the intake manifold include the compressor mass flow (entering) which is found from the compressor map; and the engine intake mass flow (leaving or entering) which is found from the reciprocator model. The mass flows entering and leaving the exhaust manifold as a whole include the turbine mass flow (leaving) which is found from the turbocharger turbine map; the engine exhaust mass flow (entering or leaving) which is found from the reciprocator model; and the wastegate mass flow (leaving).

The differential equation for the change in intake manifold temperature is derived from the generalized temperature equation applied to an open system, i.e.,

$$\dot{T}_m = \frac{1}{A}\left[\left(\frac{\dot{m}}{m}\right)_m (B - h_m) - C\dot{\phi}_m + \frac{1}{m_m}\left(\sum_j \dot{m}_j h_j - \dot{Q}\right)\right] \qquad (5\text{-}14)$$

where A, B, and C are defined in Eqs. (3-27), (3-24) and (3-28), and are calculated by the thermodynamic property routines; $\dot{Q}$ is heat transfer rate to the manifold walls; and $\dot{\phi}$ is related to $\dot{F}$ and F by Eq. (3-8).

The differential equation for the change in intake manifold pressure is derived from the generalized pressure equation applied to an open system, i.e:

$$\dot{p}_m = \frac{\rho}{\partial\rho/\partial p}\left[-\frac{1}{\rho}\frac{\partial\rho}{\partial T}\dot{T}_m + \left(\frac{\dot{m}}{m}\right)_m \frac{1}{\rho}\frac{\partial\rho}{\partial\phi}\dot{\phi}_m\right] \qquad (5\text{-}15)$$

where the density derivatives are calculated by the thermodynamic property routines.

The exhaust manifold is broken down into a series of connected open systems that are contained within the overall manifold system (see section 5.5). For these sub-systems, the pressure derivative is determined by applying the conservation equations (5-12) to (5-15) to the exhaust manifold as a whole. The exhaust ports are considered outside of the overall exhaust manifold control volume. However, the pressure derivative for the exhaust ports is set equal to that for the exhaust manifold as a whole.

The rate of change of mass within each of these sub-systems can be obtained by rearranging equation (5-15) as follows:

$$\dot{m}_i = V_i\left(\frac{\partial \rho}{\partial p}\dot{p}_i + \frac{\partial \rho}{\partial T}\dot{T}_i + \frac{\partial \rho}{\partial \phi}\dot{\phi}_i\right) \qquad (5\text{-}16)$$

where the subscript i refers to the different sub-systems of the exhaust manifold. The rate of change of temperature and composition of each section are calculated from equations (5-14) and (5-13), respectively.

The mass flow between sections of the exhaust manifold is determined by the mass flow through the exhaust valve (see section 4.1) and the rate of mass storage within any sections upstream of the section in question due to changes in the properties of those sections. For instance, the mass flow out of the port section and into the runner section is found by subtracting the change in mass in the port as found by equation (5-16) from the mass flow through the exhaust valve.

5.7 Manifold Heat Transfer

With the incorporation of an intercooler, heat transfer from the intake manifold to the environment becomes small enough to be neglected. Heat transfer from the exhaust manifold, however, is significant. Heat transfer from the gas in the exhaust manifold to the environment involves a combination

of forced convective heat transfer from the gas to the inside walls, conduction from the inside walls to the outside walls and to the water jacket, and natural (and probably forced) convection from the outer surfaces to the environment.

To determine the heat transfer in the exhaust manifold, each section is considered separately. Within each section, the gas temperature, the heat transfer coefficient, and the inside wall surface temperature are assumed to be uniform. Both the gas temperature and heat transfer coefficient are allowed to vary with time while the inside wall surface temperature is taken as constant with time. The inside wall surface temperature can be either specified as an input, or calculated from a specification of the component wall structure, in the manner described in sections 6.2.2 and 6.2.3.

5.7.1 Port heat transfer

The heat transfer in the exhaust port is highly unsteady. As the exhaust valve first comes open, a high velocity jet of high temperature gases sets up recirculation zones in the port [36] that result in a high heat transfer coefficient. When the exhaust valve is fully open, the flow resembles turbulent pipe flow and the heat transfer coefficient is diminished. Then, as the exhaust valve is going closed, there is another period when a narrow jet of gases enhances the heat transfer by setting up a recirculation zone. The valve open period is followed by a much longer period with very low mass flow and a correspondingly low heat transfer coefficient.

In order to quantify the heat transfer in the exhaust port, the results of Caton [37] are applied. Based on fine wire temperature measurements of the port gas temperature in a spark ignition engine, Caton arrived at the following correlations for the heat transfer during different phases of the exhaust valve opening:

Valve opening phase ($l/D < 0.2$):

$$Nu = 0.4\ Re_j^{0.6} \tag{5-17}$$

Valve open phase ($l/D > 0.2$):

$$Nu = 0.023\ C_R C_{EE} Re^{0.8} Pr^{0.4} \tag{5-18}$$

Valve closing phase ($l/D < 0.2$):

$$Nu = 0.5\ Re_j^{0.5} \tag{5-19}$$

Valve closed:

$$Nu = 0.023\ Re^{0.8} Pr^{0.4} \tag{5-20}$$

where Nu = Nusselt number

Pr = Prandtl number

$Re_j = \frac{V_j l}{\nu}$: Jet Reynolds number

$Re = \frac{VD}{\nu}$: Pipe Reynolds number, based on cycle-averaged mass flow

V_j = Velocity of flow through exhaust valve

V = Pipe flow velocity

l = Valve lift

D = Valve diameter

ν = Dynamic viscosity for flow

C_R = Correction factor for surface roughness

C_{EE} = Correction factor for entrance effects

Some modifications were made to these results for the present study. A correction factor was added to the correlation for the valve open phase to account for the sharp bend for an exhaust port. This factor is the correction

for bent pipes discussed in section 5.7.2. Also, during the period when the valve is closed, the mass flow is based on the instantaneous mass flow between sections instead of on the average flow over the complete cycle, as was done by Caton. For a turbocharged engine, this flow is not zero, in general, because gas flow is induced in inactive sections of the exhaust manifold by the pressure pulsations produced when other cylinders exhaust.

5.7.2 Exhaust manifold

Turbulent pipe flow correlations are usually applied to the exhaust manifold heat transfer. For fully developed pipe flow in a straight pipe with large temperature gradients, the heat transfer coefficient can be derived from the following experimental correlation that relates Nusselt, Reynolds and Prandtl numbers [35]:

$$Nu = 0.023\, Re^{0.8} Pr^{0.3} \qquad (5\text{-}21)$$

In the exhaust manifold of an engine, not all of the qualifying conditions for this equation apply. Most significantly, the flow is not fully developed, due to the short length of the pipe, and the pipe is not straight. To correct for these differences, two correction factors are introduced, based on empirical results of studies of the effects of entrance length and pipe bends on pipes.

The correction factor for entrance effects is based on the work of Boelter, Young, and Iversen [38]. They conducted experimental work on the variation of the heat transfer coefficient along the length of a tube starting at the inlet of the tube. Fitting a curve to the experimental results for a tube with an elbow at the entrance, yields the following equation for the local heat transfer coefficient:

$$C_{EE} = \frac{Nu_x}{Nu_\infty} = 2.2 \left(\frac{x}{D}\right)^{-0.3} \qquad (5\text{-}22)$$

valid for $3 < x/D < 14$

where x = entrance length

Nu_x = local Nusselt number

Nu_∞ = Nusselt number for fully developed flow.

In order to find the average correction factor for a section, equation (5-22) is integrated over the section and divided by the length of the section, leading to

$$C_{EE} = 3.1\, D^{0.3}\, \frac{(L_2)^{0.7} - (L_1)^{0.7}}{L_2 - L_1} \qquad (5\text{-}23)$$

where D = diameter of the section

L_1 = distance from the exhaust valve to the inlet of the section

L_2 = distance from the exhaust valve to the outlet of the section

The correction factor for bent pipe is based on the work of Seban and McLaughlin [39] and Rogers and Mayhew [40]. They found that the appropriate correction factor for bent pipe is:

$$C_{BP} = \frac{Nu_S}{Nu_{BP}} = \left(\frac{r}{R}\right)^{0.1} Re^{0.05} \qquad (5\text{-}24)$$

where r = Pipe radius

R = Bend radius

Nu_{BP} = Nusselt number for the bent pipe

Nu_S = Nusselt number for a straight pipe.

The Nusselt number for the bent pipe is the average of the heat transfer coefficient around the circumference of the pipe.

Combining the formula for fully developed straight pipe flow with the correction factors for entrance effects and for pipe bends gives the

correlation used for the heat transfer coefficient for sections of the pipe downstream of the port section, and for the exhaust port during the periods when the exhaust valve is fully open or closed:

$$Nu = 0.023\, C_{EE} C_{BP} Re^{0.8} Pr^{0.3} \qquad (5\text{-}25)$$

5.7.3 Connecting pipe between the turbines

The heat transfer for the connecting pipe between the turbocharger and the power turbines is treated in the same way as for the exhaust manifold. The heat transfer coefficient is based on turbulent pipe flow using equation (5-25). The overall heat transfer coefficient and the inside wall surface temperature are calculated in the manner described in sections 6.2.2 and 6.2.3.

5.8 Pressure Losses

5.8.1 General

Pressure loss terms have been included at five locations in the overall system model. These are:

between compressor discharge and intercooler inlet,

across intercooler,

between exhaust manifold and turbine inlet,

between turbine outlet and power turbine inlet,

between power turbine outlet and atmosphere.

Each of these pressure drops is calculated using the corresponding friction factors and friction coefficients for the geometry of each passage. For straight-sections:

$$\Delta P = 4f(L/D)(\rho V^2/2) \qquad (5\text{-}26)$$

where L = length of passage

D = diameter of passage

ρ = bulk density

V = average velocity

f = friction factor, which is correlated by (5-17) for the surface roughness and range of Reynolds numbers to be encountered.

Note that

$$f = 0.046/(Re)^{0.2} \qquad (5\text{-}27)$$

with $Re = \rho VD/\mu$

For bends, enlargements, contractions, etc:

$$\Delta P = K_f \rho V^2/2 \qquad (5\text{-}28)$$

where K_f = friction coefficient for a particular passage geometry. Values of K_f for typical geometries are commonly available [35].

5.8.2 Exhaust manifold and turbine connecting pipe

The pressure drop for the exhaust manifold of a 6 cylinder diesel engine was found by Primus [41] to be a factor of 10 to 15 times higher than the pressure drop calculated based on equations (5-26) and (5-27) alone. This increase in flow losses is apparently due to the complex shape of the manifold and the interaction of the flow with the open passageways from other cylinders. For this reason, equation (5-28) is used for the calculation of the exhaust manifold pressure drop with K_f left as an input parameter for the user to specify. Primus found that values of 2 to 3.5 were appropriate for his test manifold. Different values may be used for manifolds of different designs. A similar user option to input K_f for the connecting pipe between the turbine is also included in the code.

6. WALL CONDUCTION MODELS

6.1 Introduction

As described in sections 4.4 and 5.7, the heat transfer rates from the gas to the walls of the various system components depend on the instantaneous difference between the gas and the wall temperature. Estimates of these engine wall temperatures have been calculated in the past [42], [6] based on the following assumptions:

(i) each heat transfer surface of interest is at a uniform surface temperature; i.e. surface temperature variations across a particular area are neglected.

(ii) The heat transfer surface temperatures are constant with time; i.e. cycle-periodic surface temperature variations are not considered.

(iii)Heat transfer by conduction through the walls is treated on a one-dimensional basis.

The one-dimensional, uniform surface temperature model is certainly a simplification for surfaces with large temperature variations, such as piston bowls, or for surfaces with complicated heat transfer path lengths, such as the cylinder liner. Also, uniform surface temperatures are not adequate for detailed thermal stress calculations. For most surfaces, however, temperature varies much more rapidly in directions perpendicular to the surface, so that the above one-dimensional treatment is justified.

The assumption of constant wall temperatures over the engine operating cycle is reasonable for engines with high conductivity metal walls and forced convection jacket cooling. Measurements by LeFeuvre [27] and Whitehouse [43] on conventional engines have suggested that cyclic surface temperature swings are fairly small, ranging from 5 to 15 Kelvins. However, for engine surfaces insulated with low-conductivity materials, such as ceramics, surface temperature swings are expected to be more critical [44].

Figure 6 shows a typical ceramic/metal composite wall structure. The heat transfer rate from the gas to the wall is a harmonic function of time, with a period of one engine cycle. This time-dependent boundary condition will set up periodic temperature waves that will propagate into the wall structure. Because of the relatively low thermal diffusivities of ceramics, these disturbances will only penetrate a small distance from the surface of the material, beyond which the temperature distribution is steady-state.

These cyclic transients, should not be confused with engine start-up wall transients which die-away once steady-state engine operation is established. Cyclic transients are superposed on the steady-state conduction temperature profiles. Thus, their effect should be taken into account for the accurate prediction of maximum wall surface temperatures (important for lubrication considerations) and temperature distribution in the wall structures (important for material stress considerations).

Assuming uniform material properties which do not vary with temperature, the total temperature (steady plus time-periodic) $T(x,t)$, at any point x within the wall, and at any time t, will satisfy the heat conduction equation, i.e.

$$\nabla^2 T = \frac{1}{\alpha} \frac{\partial T}{\partial t} \qquad (6\text{-}1)$$

where α is the thermal diffusivity of the material. The solution to eq. (6-1) is developed in the following sections by decomposing the problem into its steady-state and time-periodic components.

6.2 Steady-State Problem

The steady-state heat transfer rate per unit inside surface area, $\dot{Q}_s$, through a composite '' structure is given by

$$\dot{Q}_s = U(\bar{T}_w - T_c) \tag{6-2}$$

where U = over-all coefficient of heat transfer based on inside surface area

$\bar{T}_w$ = steady-state inside wall surface temperature

T_c = outside wall surface temperature, coolant temperature, or ambient temperature

The cylinder head and the piston crown of the insulated engine are modelled as flat composite walls, while the cylinder liner, manifolds, and connecting ducting are modelled as cylindrical composite walls. The appropriate expressions for the over-all heat transfer coefficient and steady-state temperature distribution for these two types of wall structure are summarized in sections 6.2.1 and 6.2.2. The inside wall steady-state surface temperature is determined through a heat balance between the cycle-averaged heat transfer rate from the gas to the walls and the steady-state wall heat conduction. This involves an iterative procedure which is described in section 6.2.3.

6.2.1 Flat composite wall

The overall coefficient of heat transfer, U_p, for a flat composite wall is defined as

$$\frac{1}{U_p} = \sum_{i=1}^{n} \frac{L_i}{k_i} \tag{6-3}$$

where n = number of flat layers

L_i = thickness of i^{th} layer

k_i = thermal conductivity of i^{th} layer

If the boundary condition on the outside wall surface is specified in terms of an outside heat transfer coefficient and a coolant or ambient temperature (versus a specified outside wall temperature), a modified overall heat transfer coefficient is defined as

$$\frac{1}{U_p} = \sum_{i=1}^{n} \frac{L_i}{k_i} + \frac{1}{h_c} \tag{6-4}$$

where h_c is the heat transfer coefficient to the outside.

The steady-state temperature distribution for the i^{th} layer is obtained from the solution of Eq. (6-1) in its steady form, i.e.

$$\frac{\partial^2 T_s}{\partial x^2} = 0 \tag{6-5}$$

The boundary conditions are

$$T_s = T_s(\dot{Q}_s, x_i), \text{ at } x = x_i \tag{6-6a}$$

$$T_s = T_s(\dot{Q}_s, x_{i+1}), \text{ at } x = x_{i+1} \tag{6-6b}$$

leading to the following temperature distribution within the i^{th} layer

$$T_s(x) = [T_s(x_{i+1}) - T_s(x_i)]\frac{(x-x_i)}{L_i} + T_s(x_i) \tag{6-7}$$

6.2.2 Cylindrical composite wall

The overall coefficient of heat transfer, U_c, based on the inside surface area of a cylindrical wall structure is defined as

$$\frac{1}{r_1 U_c} = \sum_{i=1}^{m} \frac{\ln(r_{i+1}/r_i)}{k_i} \tag{6-8}$$

where m = number of cylindrical layers

r_i = inside radius of i^{th} layer

r_{i+1} = outside radius of i^{th} layer

k_i = thermal conductivity of i^{th} layer

Again, if the outside boundary condition involves the heat transfer coefficient to the outside, the overall heat transfer coefficient is modified as follows:

$$\frac{1}{r_1 U_c} = \sum_{i=1}^{m} \frac{\ln(r_{i+1}/r_i)}{k_i} + \frac{1}{r_{m+1} h_c} \tag{6-9}$$

where r_{m+1} = outside radius of m^{th} layer

h_c = heat transfer coefficient to the outside

The steady-state temperature distribution for the i^{th} layer is obtained from solution of equation (6-1) in its steady form, i.e.

$$\frac{1}{r}\frac{\partial}{\partial r}\left(r\frac{\partial T_s}{\partial r}\right) = 0 \tag{6-10}$$

The boundary conditions are

$$T_s = T_s(\dot{Q}_s, r_i) \text{ , at } r = r_i \tag{6-11a}$$

$$T_s = T_s(\dot{Q}_s, r_{i+1}) \text{ , at } r = r_{i+1} \tag{6-11b}$$

leading to the following temperature distribution within the i^{th} layer

$$T_s(r) = (T_s(r_i) - T_s(r_{i+1}))\frac{\ln(r/r_{i+1})}{\ln(r_i/r_{i+1})} + T_s(r_{i+1}) \tag{6-12}$$

6.2.3 Determination of steady-state inside wall surface temperature

The steady-state inside wall surface temperatures of each of the engine components is not known a priori. At the start of the cycle simulation,

approximate estimates of these temperatures are assumed. Based on these estimates, the instantaneous heat transfer rates, convective and radiative, to the combustion chamber walls are calculated throughout the cycle. At the end of the cycle, a heat balance is performed between the cycle-averaged gas/wall heat transfer rate and the heat conducted through the walls of each component to compute a new surface temperature. These new temperatures are used in the next cycle iteration, until the calculation converges. Details of the heat balance follow.

The instantaneous heat transfer rate to the combustion chamber walls is calculated from

$$\dot{Q}_w(t) = h(t)(T_g(t) - \bar{T}_w) \tag{6-13}$$

where $\bar{T}_w$ = inside wall temperature at cycle start

$T_g(t)$ = instantaneous gas temperature

$h(t)$ = instantaneous heat transfer coefficient

During combustion, $h(t)$ is replaced by an effective linearized heat transfer coefficient $h_{eff}(t)$, given by Eq. (D-7), to take into account the effects of radiation on the total heat transfer rate.

The cycle-averaged gas/wall heat transfer rate is given by

$$\dot{Q}_w = \frac{\int h(t)(T_g(t) - \bar{T}_w)dt}{\int dt} \tag{6-14}$$

where $\int$ denotes integration over the complete cycle. Equation (6-14) can be rewritten as

$$\dot{Q}_w = \overline{h\,T_g} - \bar{T}_w\bar{h} \tag{6-15}$$

where the bar denotes cycle-averaged.

The steady-state heat transfer rate conducted through a composite wall structure was expressed by equation (6-2), involving an over all wall heat transfer coefficient. Combining equations (6-2) and (6-15), an updated wall temperature can be computed according to

$$\bar{T}'_w = \frac{\overline{h}\,\overline{T}_g + UT_c}{\overline{h} + U} \tag{6-16}$$

where the prime denotes the temperature to be used in the next cycle iteration. The calculation is repeated until the new wall temperature is within a certain percentage of its value at the end of the previous cycle.

6.3 Time-Periodic Problem

6.3.1 Formulation of finite difference scheme

The time-periodic part, $T_p(x,t)$, of the temperature distribution within any parallel slab will satisfy the unsteady conduction equation, i.e.,

$$\frac{\partial^2 T_p}{\partial x^2} = \frac{1}{\alpha}\frac{\partial T_p}{\partial t} \tag{6-17}$$

In order to solve this continuous partial differential equation, a finite difference technique will be used. The slab is modeled by a number of N discrete nodal points, x_i. At each node, the finite-difference approximation to the governing equation provides an algebraic equation connecting the instantaneous nodal temperature to those at the surrounding nodes.

The finite difference schemes which have been used to solve partial differential equations of the form of Eq. (6-17), can be grouped into two general categories: explicit and implicit [45]. In explicit schemes, the instantaneous value of the variable at any node is given by the values of the

variable at the node and its neighboring nodes calculated from the previous time step. These schemes are fairly simple, and computationally very efficient. However, they are stable only under certain conditions and are limited to uniformly-spaced discrete nodes. On the other hand, implicit schemes are unconditionally stable, and some can handle arbitrarily spaced discrete nodes. From the computational point of view, though, implicit schemes are very intensive. Since the instantaneous value of a nodal variable depends on the neighboring values of the variable at the current and previous time steps, these schemes, unfortunately, involve large matrix inversions.

For the purposes of the current work, it is desired to calculate the temperature distribution within the walls of the engine combustion chamber in parallel with the engine simulation calculation. Thus, special effort was made to develop a numerical scheme that would be:

(i) least demanding in computer time

(ii) able to handle arbitrarily-spaced discrete nodes, so as to maximize the accuracy of the solution within the relatively thin penetration depth of the cyclic engine transients

(iii) stable.

To satisfy all the above requirements, an Euler explicit scheme was suitably modified, by mapping the arbitrarily-spaced discrete noues x_i of the desired solution domain into corresponding uniformly-spaced nodes y_i, according to the following transformation:

$$y = \frac{a + bx}{1 + cx} \tag{6-18}$$

This transformation w s selected because of its following merits [46]:

(i) three of the nodes x_i can be mapped into three specified nodes y_i.

(ii) all other nodes x_i are then mapped smoothly in between the three specified nodes y_i.

(iii) the transformation is differentiable up to any order.

Using (6-18), Eq. (6-17) can take the following form for each node x_i:

$$\left(\frac{\partial y}{\partial x}_i\right)\left[\frac{\partial}{\partial y}\left(\frac{\partial T}{\partial x}\right)\right]_i = \frac{1}{\alpha}\left(\frac{\partial T}{\partial t}\right)_i \tag{6-19}$$

By approximating the derivative with respect to y through finite differences, and recalling (6-18), Eq. (6-19) can be re-written as

$$\left(\frac{1}{\Delta y}\right)\left(\frac{\partial y}{\partial x}_i\right)\left[\left(\frac{\partial y}{\partial x}\right)_{i+1/2}\left(\frac{\partial T}{\partial y}\right)_{i+1/2} - \left(\frac{\partial y}{\partial x}\right)_{i-1/2}\left(\frac{\partial T}{\partial y}\right)_{i-1/2}\right] = \frac{1}{\alpha}\left(\frac{\partial T}{\partial t}_i\right) \tag{6-20}$$

where Δy is the uniform spacing between two adjacent nodes in the transformed coordinate system.

Once again, by taking finite difference expressions for the derivatives with respect to y, and after some rearrangement, we get

$$T_i = T_i^{\circ} + \frac{DYDXM}{CN}\left[DYDXR\left(T_{i+1}^{\circ} - T_i^{\circ}\right) - DYDXL\left(T_i^{\circ} - T_{i-1}^{\circ}\right)\right] \tag{6-21}$$

where $DYDXM = \left(\frac{\partial y}{\partial x}\right)_i$ (6-22a)

$$DYDXR = \left(\frac{\partial y}{\partial x}\right)_{i+1/2} \tag{6-22b}$$

$$DYDXL = \left(\frac{\partial y}{\partial x}\right)_{i-1/2} \tag{6-22c}$$

$$CN = \frac{\Delta y^2}{\alpha \Delta t} : \text{Courant number} \tag{6-23}$$

and the superscript ° denotes temperature values at the previous time step. Note that the method is stable provided that [47]

$$CN \geq 2 \tag{6-24}$$

For time-step sizes of the order of one engine crank angle, and material diffusivities in the range of 10^{-5} to 10^{-6} m^2/s (most materials of interest), this condition will be satisfied for nodal spacings as small as 1/10 to 1/100 of a mm.

6.3.2 Application of finite difference scheme

The finite difference scheme was applied to calculate the periodic temperature distribution in the two parallel layer wall structure (piston or head), shown in Fig. 6. In general, under typical engine operating conditions, the cyclic transients do not penetrate into the wall structure for a distance greater than a few mm (and thus will not extend into the second layer). However, to maximize the flexibility of the code to analyze even thin coatings (of order of a mm), the code is set-up with a capability to calculate transients over the entire wall region. Obviously, more nodes should be placed in the first layer than in the second one.

For the first layer, the transformation (6-18) is introduced, so that

$x = -L_1$ maps into $y = 0$

$x = 0$ maps into $y = 1$

$x = -L_1 + \delta$ maps into $y = F$

with $F = 0.4$ to 0.5, meaning that 40 to 50 percent of the nodes x_i are placed within a distance of the order of the penetration depth δ in the first layer. These three conditions determine a, b, c in Eq. (6-18). Then, the temperature $T_{1,i}$ at any node i of the first layer, can be calculated from Eq. (6-21).

For the second layer, a relatively small number of uniformly-spaced nodes is sufficient. Then, with $y = x$, Eq. (6-21) for the temperature $T_{2,j}$ at any node j of the second layer, simplifies to the following standard form [47]:

$$T_{2,j} = \frac{T^{\circ}_{2,j-1} + (CN-2)T^{\circ}_{2,j} + T^{\circ}_{2,j+1}}{CN} \qquad (6\text{-}25)$$

Note again that for stability, $CN \geq 2$. (The limit $CN = 2$ would imply that the local node temperature has no effect on its future value).

At the interface between the two layers (x=0), continuity of temperature and heat flux leads to the following boundary conditions:

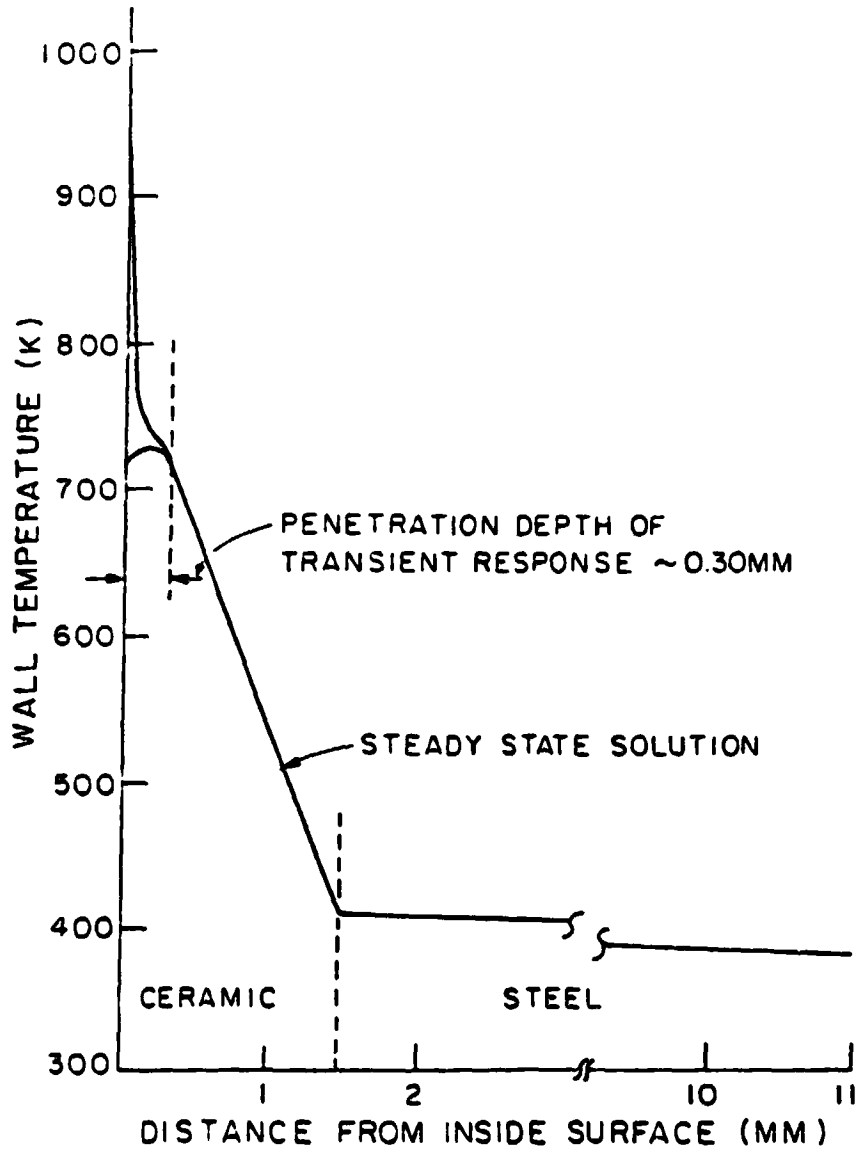

Fig. 6: Typical temperature within a ceramic/metal composite wall structure in the engine combustion chamber.

$$T_{1,N} = T_{2,1} \tag{6-26}$$

where N is number of nodes in first layer, and

$$k_1\left(\frac{\partial T}{\partial x}\right)_{x=0-} = k_2\left(\frac{\partial T}{\partial x}\right)_{x=0+}$$

or, introducing transformation (6-18) in the first layer, and aproximating the derivatives through finite differences, we get

$$k_1\left(\frac{\partial y}{\partial x}\right)_0 \frac{3T_{1,N} - 4T_{1,N-1} + T_{1,N-2}}{\Delta y} = k_2 \frac{-3T_{2,1} + 4T_{2,2} - T_{2,3}}{\Delta x_2} \tag{6-27}$$

where Δy was defined in Eq. (6-20) and Δx_2 is the uniform spacing between two adjacent nodes in the second layer.

To validate the numerical scheme and to optimize the number and spacing of nodal points, the method was applied to calculate the temperature distribution in a two layer composite, slab subject to a harmonically varying gas temperature at $x = -L_1$, and a constant ambient temperature at $x = L_2$. The exact solution was also obtained analytically for the same problem [10]. The approximate results were shown to be in excellent agreement with the exact results for a range of different materials and wall structures [10].

6.4 Combined Solution

The total temperature distribution in each layer can be obtained by superposing the steady-state solution given by Eq. (6-7), and the time-periodic solution, given by Eqns. (6-21) and (6-25). The total temperature $T(x,t)$ must satisfy the full boundary conditions at the inside and outside wall surfaces.

At the hot gas side ($x = -L_1$),

$$-k_1\left(\frac{\partial T}{\partial x}\right)_{x=-L_1} + \dot{Q}_s = h_g(T_g - T_w) \tag{6-28}$$

where Q_s is the steady-state heat flux given by (6-2), h_g is an effective linearized coefficient (convective and radiative) defined by (D-7), and

$$T_w = \bar{T}_w + T_{1,1} \tag{6-29}$$

Introducing finite-difference approximations, (6-28) can be rewritten as

$$- k_1 \left(\frac{\partial y}{\partial x}\right)_{-L_1} \frac{3T_{1,1} - 4T_{1,2} + T_{1,3}}{2\Delta y} + \dot{Q}_s = h_g (T_g - T_w) \tag{6-30}$$

Similar equations apply for the boundary condition at the ambient or coolant side ($x = L_2$), where either the total heat flux or the total wall temperature can be prescribed.

The calculation is staged as follows. First, the steady-state solution for the temperature distribution within each component wall and the average heat flux conducted through each wall are obtained by following the iteration procedure described in section 6.2.3, i.e. assuming no cyclic transients. Once the steady-state heat flux is obtained, the transient calculation is performed by applying the finite difference scheme and the total boundary conditions (6-28) and (6-30).

7. METHOD OF SOLUTION AND PROGRAM INPUTS AND OUTPUTS

7.1 Basic Method of Solution

The conservation equations of mass and energy for the contents of an open thermodynamic system are applied in turn to the master reciprocating cylinder, the intake manifold, and the series of exhaust manifold sections. Further, the individual submodels of the various system components and their thermodynamic and heat transfer processes are brought together to form a complete system model. The result is a set of simultaneous first-order ordinary differential equations. To perform predictive calculations with the cycle simulation, these equations must be integrated simultaneously over the full operating cycle. Note, however, that some of the governing equations like the mass flow rate through the intake or the exhaust valve, the non-dimensional fuel burning rate, etc. apply only during parts of the cycle.

Integration of the governing equations is performed numerically using a standardized code developed by Shampine and Gordon [48]. The method is based on a predictor-corrector technique that uses a modified divided difference form of the Adams Pece formulas. The code adjusts its order and step size internally to maximize efficiency and control the local error per unit step in a generalized sence. Detailed documentation of the integration routine is provided in the listing of the code.

A flow chart showing the overall structure of the entire system simulation is shown in Figure 7. After the initialization of the state variables, the program proceeds with the simultaneous integration of the governing system equations. The latter can be grouped into two major subsets: equations describing the thermodynamic processes in the master cylinder of the reciprocator; and equations associated with other components in the system (manifolds, turbocharger, etc.) that have inherent multi-cylinder

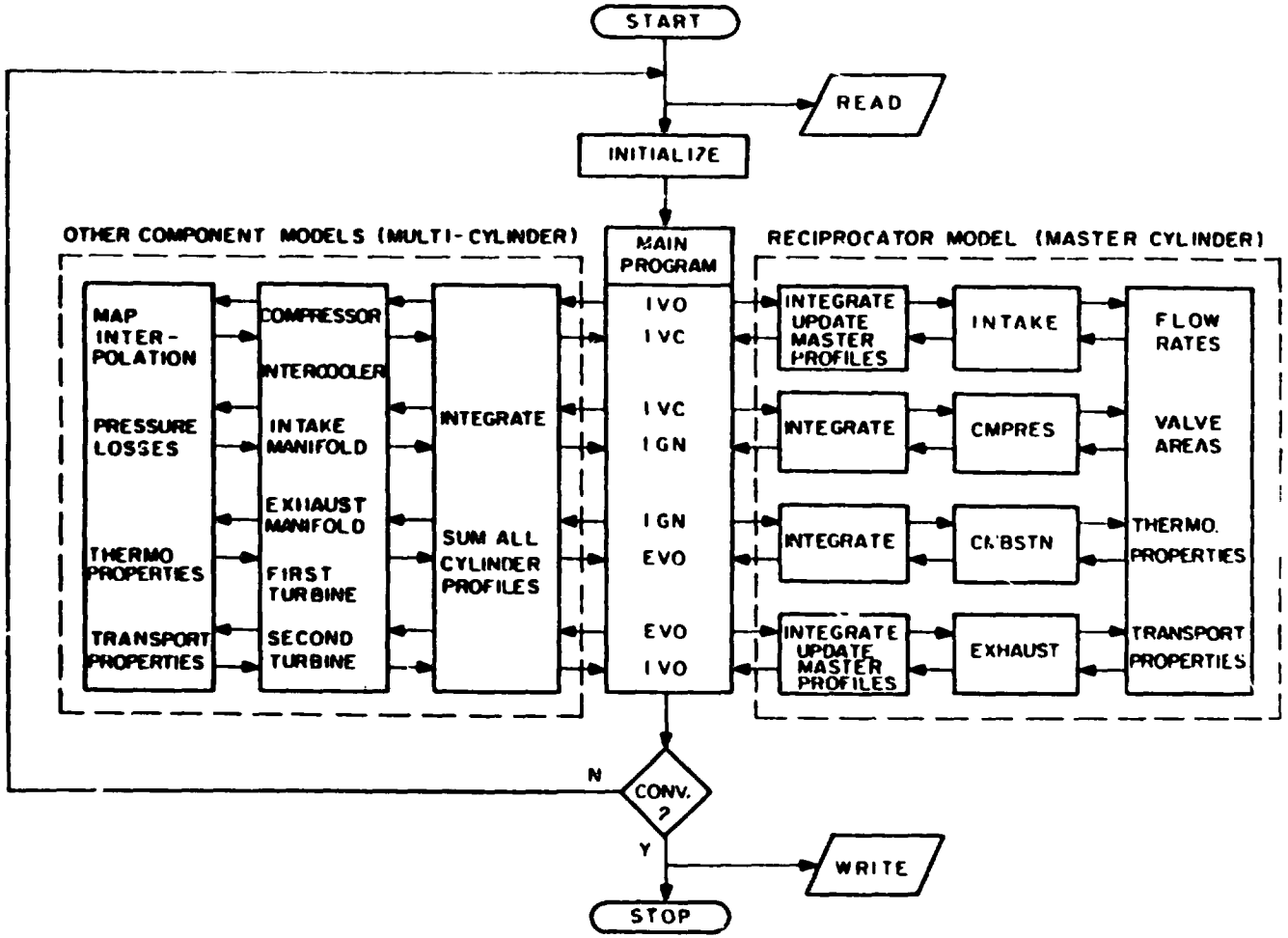

Fig. 7: Flow chart of simulation program.

capability. The main program determines which equations in each sub-set will be passed to the integrator, couples the two sub-sets and transfers information across them, and prints out results as the cycle proceeds.

On the reciprocator model side, the main program passes to the integrator different subroutines corresponding to the intake, compression, combustion and exhaust processes of the master cylinder, as the engine cycle proceeds. On the other components side, the main program supplies the integrator with the same set of governing equations for the manifolds, turbocharger, etc. throughout the cycle. Appropriate utility routines, are called by the major routines to help in the evaluation of the necessary derivatives at each step. These include routines to calculate the steady-state and cyclic periodic temperature profiles within the various component wall structures, routines to calculate mass flow rates through valves and interpolate valve area tables (called by the intake and exhaust routines), routines to interpolate turbomachinery maps and predict the heat transfer and pressure losses in the ducting (called by the other components routine), and thermodynamic and transport property routines (called by all major routines).

The mass flow rate and enthalpy flux profiles of the master cylinder, generated by the simulation during the intake and the exhaust processes, are stored in the main program. Using this information, the main program calls a subroutine that:

i) generates the profiles of all the other cylinders as echoes of the master cylinder profiles;

ii) sums the intake and exhaust profiles contributed by each cylinder at every instant to give total reciprocator mass and enthalpy flows, etc. The resultant profiles are communicated from the main program to the other components routine throughout the engine cycle.

Approximate estimates of all state variables are assumed, initially. More than one iteration is generally required to model system operation under steady conditions. The integration continues until the system reaches a quasi-steady condition, defined as the condition in which the value of each state variable at a particular crank-angle is within a specified interval of its value at that crank-angle in the previous engine cycle.

7.2 Program Inputs and Outputs

The input parameters which must be specified for each cycle simulation calculation include the following groups: system operating mode, system operating conditions, system dimensions and design parameters, parameters for the wall conduction models, empirical parameters for the various simulation sub-models, initial conditions of the system and certain computational parameters.

From this information, the simulation program can predict the performance of the total engine system under a wide range of operating conditions. The output includes mean engine performance parameters, such as power, specific fuel consumption, mean effective pressure, thermal efficiency, etc., as well as detailed information about the state of the total system as a function of crank-angle throughout each engine cycle.

7.2.1 Inputs

I. System operating mode

In order to maximize the flexibility of the code to handle different system configurations, and assess the effect of different modeling assumptions on system performance, the user is provided with a choice of several options:

a. The system can be turbocharged and turbocompounded, or turbocharged only.

b. The steady-state inside wall surface temperatures of the piston, cylinder head, cylinder liner, manifolds, and turbine connecting pipe can be specified as an input, or calculated from a specification of the component wall structure.

c. Additionally. the time-dependent temperature distribution in the piston and cylinder head can be computed using a one-dimensional unsteady finite difference model for the component wall.

d. The ignition delay period can be predicted based on our ignition delay model, or can be specifed based on experimental data.

e. Either the commonly used Annand's radiation model, or the flame radiation model developed here can be used to predict instantaneous radiative heat transfer rates.

II. System operating conditions

a. Reciprocator speed (RPM)

b. Mass of fuel injected per cycle

c. Injection timing

d. Fuel parameters

e. Steady-state inside wall surface temperatures of piston, cylinder head, cylinder liner, manifold walls, and turbine connecting pipe (for specified wall temperature option only)

f. Power turbine gear ratio

III. System dimensions and design parameters

1. Reciprocator Parameters

   a. Number of cylinders

   b. Cylinder bore

c. Cylinder stroke

d. Connecting rod length

e. Clearance volume

f. Valve timings (crank angles at which the intake and exhaust valves open and close)

g. Tabulated values for the effective valve open areas (including discharge coefficient effects)

ii. Other Component Dimensions

a. Intake and exhaust manifold dimensions

b. Turbine connecting pipe dimensions

iii. Intercooler Characteristics

a. Coolant flow heat capacity

b. Heat exchange surface area

c. Over-all heat transfer coefficient

iv. Turbomachinery Parameters

a. Compressor, turbocharger turbine and power turbine maps

b. Turbocharger rotational inertia

c. Turbocharger rotational damping

d. Power turbine transmission efficiency

IV. Wall conduction model parameters

These parameters need to be specified when it is desired to predict the steady-state and transient (for piston and cylinder head only) temperature distribution within the various system component walls. For each material layer of the piston, cylinder head, liner, manifold sections and turbine connecting pipe, the wall structure specifications include:

a. Thickness

b. Inside wall radius (cylindrical components only)

c. Thermal conductivity

d. Thermal diffusivity (piston and head only)

For each component, the boundary conditions on the outside wall surface must be specified, i.e.:

a. Ambient (or coolant) temperature, and heat transfer coefficient from the outside wall surface to the ambient (or coolant), or

b. specified wall temperature on outside surface

Finally, for the finite difference scheme applied to the unsteady conduction through the piston and cylinder wall, the following are required

a. Number of nodes placed within each layer of a given component

b. Fraction of nodes of first layer placed within the penetration depth of cyclic engine transients.

V. Other sub-model empirical parameters

a. Ignition delay correlation constants; e.g., (4-12)

b. Burning rate distribution constants; e.g., (4-7), (4-8), (4-9)

c. Nu-Re number correlation constants, appropriate for the reciprocator cylinder, exhaust port, manifolds, and turbine connecting pipe; Equations (4-17), and (5-17) up to (5-21)

d. Turbulent dissipation constant; Eq. (4-34)

e. Annand's radiation model calibrating constant

f. Friction model constants; e.g., (4-48).

IV. Initial conditions

a. Cylinder pressure, temperature, and composition

b. Intake manifold pressure, temperature, and composition

c . Exhaust manifold pressure, temperature, and composition

d. Turbocharger speed

VII. Ambient conditions

a. Intake temperature

b. Intake pressure

c. Final exhaust pressure

VIII. Computational parameters

a. Convergence margins for each state variable

b. Error tolerances for integration of the differential equations

c. Other parameters used in the integration algorithm "ODERT" (For a detailed description of these parameters, see the engine simulation code.)

7.2.2 Outputs

Four types of outputs are generated by the cycle simulation:

I. Input echo

A listing of all the input parameters, including some quantities derived directly from the given inputs (e.g. engine displacement and compression ratio).

II. Major crank-angle by crank angle results

At specified crank-angle intervals, the values of the following state variables are returned:

a. Cylinder pressure, temperature, and average equivalence ratio

b. Intake manifold pressure, temperature and average equivalence ratio

c. Exhaust manifold pressure, temperature and average equivalence ratio

In addition, the following other quantities are reported at the same intervals:

a. Heat transfer model results (such as heat transfer rates from gas to various component wall surfaces, instantaneous convective heat transfer coefficient, temperature profiles within various component wall structures)

b. Turbulent flow model results (such as mean flow velocity, turbulent intensity, macroscale of turbulence)

c. Code which monitors the performance of the integration routine.

Integrating through the different processes for the master cylinder, the following quantities are reported during the corresponding process:

i. Intake

a. Mass flow through intake valve

b. Mass flow through exhaust valve

c. Velocity through intake valve

d. Velocity through exhaust valve

ii. Combustion

a. Non-dimensional fuel burning rate

b. Fuel burnt as a function of total fuel injected

c. Flame radiation model results (such as radiant heat transfer, radiant temperature, adiabatic flame temperature, emissivity)

iii. Exhaust

a. Mass flow rate through exhaust valve

b. Velocity through exhaust valve

III. Integrated results and cycle performance

After completion of an engine cycle, a summary of results obtained by integrating some of the governing equations over the cycle is given. Integrated results include the following:

a. Reciprocator thermal efficiency (gross indicated and brake)

b. Overall system brake thermal efficiency

c. Specific fuel consumption (reciprocator and overall)

d. Volumetric efficiency (based on manifold and ambient conditions)

e. Gross indicated, pumping, friction, and mean brake effective pressures

f. Total heat loss (as a fractoin of the fuel energy input)

g. Mean exhaust temperature

h. Mass of air inducted per cycle

i. Ignition delay period

j. Total heat and work transferred during each process

k. Results of an overall energy balance

IV. Sub-model results

After the overall cycle results are listed, detailed results for the main sub-models of the cycle simulation are given at specified crank angle intervals. These quantities include the following:

a. Total engine intake and exhaust mass flow rates

b. Compressor, turbocharger turbine and power turbine speed, mass flow rate, pressure ratio and efficiency

c. Power turbine work transfer

d. Pressures and temperatures at various system locations

e. Intake manifold, exhaust manifold, and turbine connecting pipe heat transfer data

f. Intercooler performance data

8. REFERENCES

1. Katz, N.R. and Lenoe, E.M., "Ceramics for Diesel Engines: Preliminary Results of a Technology Assessment," Progress Report DOE/AMMRC IAG DE-AE 101-77 CS51017, 1981.

2. Kamo, R. and Bryzik, W., "Adiabatic Turbocompound Engine Performance Predictions," SAE Paper 780068, 1978.

3. Kamo, R. and Bryzik, W., "Cummins-TARADCOM Adiabatic Turbocompound Engine Program," SAE paper 810070, 1981.

4. Assanis, D.N., Ekchian, J.A., Heywood, J.B. and Replogle, K.K., "Computer Simulation of the Heavy-Duty Turbocompounded Diesel Cycle for Studies of Engine Efficiency and Performance," DOE/NASA 0394-1, NASA CR-174755, U.S. Department of Energy, Conservation and Renewable Energy, Office of Vehicle and Engine R&D, May 1984.

5. Assanis, D.N., Ekchian, J.A., Heywood, J.B. and Replogle, K.K., "Computer Simulation of the Turbocompounded Diesel Engine System," SAE Paper from P-155, Proceedings of the Twenty-Second Automotive Development Contractor's Coordination Meeting, pp. 297-316, Dearborn, Michigan, October 29 - November 2, 1984.

6. Watson, N. and Janota, M.S., Turbocharging the Internal Combustion Engine, John Wiley & Sons, New York, 1982.

7. Lyn, W.T., "Study of Burning Rate and Nature of Combustion in Diesel Engine," IX Symposium (International) on Combustion, Proceedings, pp. 1069-1082, The Combustion Institute, 1962.

8. Shipinski, J., Uyehara, O.A. and Myers, P.S., "Experimental Correlation Between Rate-of-Injection and Rate-of-Heat-Release in a Diesel Engine," ASME Paper 68-DGP-11, 1968.

9. Watson, N., Pilley, A.D. and Marzouk, M., "A Combustion Correlation for Diesel Engine Simulation," SAE Paper 800029, 1980.

10. Assanis, D.N., "A Computer Simulation of the Turbocharged Turbocompounded Diesel Engine System for Studies of Low Heat Rejection Engine Performance," Ph.D. Thesis, M.I.T., September 1985.

11. Igura, S., Kadota, T., Hirozasu, H., "Spontaneous Ignition Delay of Fuel Sprays in High Pressure Gaseous Environment," Jap. Soc. Mech. Engrs., Vol. 41, No. 345, p. 1559, 1975.

12. Stringer, F.W., Clarke A.E., Clarke, J.S., "The Spontaneous Ignition of Hydrocarbon Fuels in a Flowing System," Proc. Auto. Div., Institution of Mech. Eng., 1970.

13. Spadaccini, L.J. and TeVelde, J.A., "Autoignition Characteristics of Aircraft-Type Fuels," United Technologies Research Center, NASA report CR-159886, 1980.

14. Hardenberg, H.O. and Hase, F.W., "An Empirical Formula for Computing the Pressure Rise Delay of a Fuel from its Cetane Number and from the Relevant Parameters of Direct-Injection Diesel Engines," SAE paper 790493, SAE Trans., Vol. 88, 1979.

15. Dent, J.C. and Mehta, P.S., "Phenomenological Combustion Model for a Quiescent Chamber Diesel Engine," SAE Paper 811235, 1981.

16. Woschni, G., "A Universally Applicable Equation for the Instantaneous Heat Transfer Coefficient in the Internal Combustion Engine," SAE Paper 670931, SAE Trans., Vol. 76, 1967.

17. Annand, J.D., "Heat Transfer in the Cylinders of Reciprocating Internal Combustion Engines," Proceedings Institute of Mechanical Engineers, Vol. 177, No. 36, 1963.

18. Annand, J.D. and Ma, T.H., "Instantaneous Heat Transfer Rates to the Cylinder Head Surface of a Small Compression-Ignition Engine," Proceedings Institute of Mechanical Engineers, Vol. 185, Second Paper, No. 72, 1971.

19. Sitkei, G., Heat Transfer and Thermal Loading in Internal Combustion Engines, Akademiai Kiade, Budapest, 1974.

20. Kamel, M. and Watson, N., "Heat Transfer in the Indirect Injection Diesel Engine," SAE Paper 790826, 1979.

21. Oguri, T. and Shigewo, I., "Radiant Heat Transfer in Diesel Engines," SAE paper 720023, SAE Trans., Vol. 81, 1972.

22. Kunitomo, T., Matsuoka, K. and Oguri, T., "Prediction of Radiative Heat Flux in a Diesel Engine," SAE Paper 750786, SAE Trans., Vol. 84, 1975.

23. Ebersole, G.D., Myers, P.S., and Uyehara, O.A., "The Radiant and Convective Components of Diesel Engine Heat Transfer," SAE Paper 701C, 1963.

24. Sitkei, G. and Ramanaiah, G.V., "A Rational Approach for Calculation of Heat Transfer in Diesel Engines," SAE Paper 720027, 1972.

25. Overtve, V.D., Bennethum, J.E., Uyehara, O.A., and Myers, P.S., "Unsteady Heat Transfer in Engines," SAE Transactions, Vol. 69, 1961, pp. 461-494.

26. Dent, J.C. and Suliaman, S.J., "Convective and Radiative Heat Transfer in a High Swirl Direct Injection Diesel Engine," SAE Paper 770407, 1977.

27. LeFeuvre, T., Myers, P.S. and Uyehara, O.A., "Experimental Instantaneous Heat Fluxes in a Diesel Engine and Their Correlation," SAE Paper 690464, 1969.

28. Flynn, P., Mizusawa, M., Uyehara, O.A. and Myers, P.S., "An Experimental Determination of the Instantaneous Potential Radiant Heat Transfer Within an Operating Diesel Engine," SAE Paper 720022, 1972.

29. Hottel, H.C. and Broughton, F.P., "Determination of True Flame Temperature and Total Radiation from Luminous Gas Flames," Industrial and Engineering Chemistry, Analytical Edition, Vol. 41932, pp. 166-175.

30. Svehla, R.A. and McBride, B.J., "Fortran IV Computer Program Calculations of Thermodynamic and Transport Properties of Complex Chemical Systems," NASA Technical Note, NASA TN D-7056, 1973.

31. Mansouri, S.H., Heywood, J.B. and Radhakrishnan, K., "Divided-Chamber Diesel Engines, Part 1: A Cycle-Simulation which Predicts Performance and Emissions," SAE Paper 820273, SAE Trans., Vol. 91, 1982.

32. Poulos, S.G. and Heywood, J.B., "The Effect of Chamber Geometry on Spark-Ignition Engine Combustion," SAE paper 830334, SAE Trans., Vol. 92, 1983.

33. Tennekes, M. and Lumley, J.L., A First Course in Turbulence, M.I.T. Press, Cambridge, Mass., 1972.

34. Millington, B.W. and Hartles, E.R., "Frictional Losses in Diesel Engines," SAE paper 680590, SAE Trans., Vol. 77, 1968.

35. Rohsenow, W.M. and Choi, H.Y., Heat, Mass, and Momemtum Transfer, Prentice-Hall, Englewood Cliffs, N.J., 1961.

36. Oldfield, S.G., and Watson, N., 'Exhaust Valve Geometry and Its Effect on Gas Velocity and Turbulence in an Exhaust Port', SAE 830151, 1983.

37. Caton, J.A., and Hewyood, J.B., "Models for Heat Transfer, Mixing and Hydrocarbon Oxidation in an Exhaust Port of a Spark-Ignition Engine', SAE Paper 800290, 1980.

38. Boelter, Young, and Iversen, NACA, TN 1451, 1948.

39. Seban, R.A., and McLaughlin, E.F., 'Heat Transfer in Tube Coils', Int. J. Heat-Mass Transfer, Vol. 6, 387-395, 1963.

40. Rogers, C.F., and Mayhew, Y.R., 'Heat Transfer and Pressure Loss in Helically Coiled Tubes', Int. J. Heat-Mass Transfer, Vol. 7, 1207-1216, 1964.

41. Primus, R.J., 'A Second Law Approach to Exhaust System Optimization', SAE 840033, 1984.

42. Streit, E. and Borman, G., "Mathematical Simulation of a Large Turbocharged Two-Stroke Diesel Engine, SAE Ppaer 710176, 1971.

43. Whitehouse, N.D., "Heat Transfer in a Quiescent Chamber Diesel Engine," Proceedings Institute of Mechanical Engineers, Vol. 185, First Paper, No. 72, 1971.

44. Morel, T. and Keribar, R., "A Model for Predicting Spatially and Time Resolved Convective Heat Transfer in Bowl-in-Piston Combustion Chambers," SAE Paper 850204, 1985.

45. Crandall, S.H., Engineering Analysis: A Survey of Numerical Procedures, McGraw-Hill, 1956.

46. Levinson, N. and Redheffer, R., Complex Variables, Holden'day Inc., 1970.

47. Dusinberre, G.M., Numerical Analysis of Heat Flow, McGraw-Hill, New York, 1949.

48. Shampine, L.F. and Gordon, M.K., Computer Solution of Ordinary Differential Equations: The Initial Value Problem, Freeman, 1974.

49. Hires, S.D., Ekchian, A., Heywood, J.B., Tabaczynski, R.J. and Wall, J.C., "Performance and NO_x Emissions Modelling of a Jet Ignition Prechamber Stratified Charge Engine," SAE Paper 760161, 1976.

50. Martin, M.K. and Heywood, J.B., "Approximate Relationships for the Thermodynamic Properties of Hydrocarbon-Air Combustion Products," Combustion Science and Technology, Vol. 15, pp. 1-10, 1977.

51. Mansouri, S.H. and Heywood, J.B., "Correlations for the Viscosity and Prandtl Number of Hydrocarbon-Air Combustion Products," Combustion Science and Technology, Vol. 23, pp. 251-256, 1980.

52. Rossini, F.D., Pitzer, K.S., Arnelt, R.L., Braun, R.M. and Primentel, G.C., Selected Values of Physical and Thermodynamic Properties of Hydrocarbons and Related Compounds, Carnegie Press, Pittsburgh, PA, 1953.

53. Stull, D.R. and Prophet, H., JANAF Thermochemical Tables, Second Edition, National Bureau of Standards Publication, NSRDS-NBS 37, 1971.

APPENDIX A

Thermodynamic Properties

Our thermodynamic model assumes that the various open systems contain mixtures of air and combustion products throughout the total engine system. By utilizing the concept of the instantaneous average equivalence ratio defined in Section 4.1, the contents of any open system can be represented as one continuous medium. Furthermore, assuming ideal gas behavior and thermodynamic equilibrium, the instantaneous gas properties can be determined from a knowledge of pressure, temperature and average equivalence ratio in the open system.

When the temperature of the cylinder contents is below 1000 K, they are treated as a homogeneous mixture of non-reacting ideal gases, their properties being calculated using the procedure outlined below [49]:

The hydrocarbon-air combustion reaction is written as:

$$\varepsilon\phi\ CH_y + O_2 + \psi\ N_2 \rightarrow x_1\ CO + x_2 H_2O + x_3 CO + x_4 H_2 + x_5 O_2 + \psi N \qquad (A\text{-}1)$$

where ψ = the molar N:O ratio of the products,

y = the molar H:C ratio of the fuel,

ϕ = the average equivalence ratio,

x_i = moles of species i per mole of O_2 reactant

and $\varepsilon = 4/(4+y)$ (A-2)

The quantities x_i are determined by using the following assumptions:

a) for lean mixtures ($\phi \leq 1$) H_2 can be neglected.

b) for rich mixtures ($\phi > 1$) O_2 can be neglected.

c) for rich mixtures, the gas water reaction

$$CO_2 + H_2 \rightarrow CO + H_2O$$

is in equilibrium with equilibrium constant K(T).

The solution for the x_i is shown in Table A-1, where C is obtained by solving equation (A-3) for its positive root.

$$(1 - K)C^2 + 2[1 - \varepsilon\phi + K(\phi - 1 + \varepsilon\phi)]C - 2K\varepsilon\phi(\phi - 1) = 0 \qquad \text{(A-3)}$$

The value of K(T) is obtained by curve fitting JANAF table data over the temperature range 400 to 3200 K and is given by

$$\ln(K(T)) = 2.743 - 1.761/t - 1.611/t^2 + .2803/t^3 \qquad \text{(A-4)}$$

where $t = T/1000$, and T is the temperature in Kelvins.

If the grams of products per mole of O_2 reactant is expressed as

$$M = (8\varepsilon + 4)\phi + 32 + 28\psi \qquad \text{(A-5)}$$

the specific enthalpy h and the specific heats at constant pressure and constant composition, c_p and c_ϕ respectively, can be expressed by the following relationships:

$$h = \frac{1}{M} \sum_{i=1}^{6} x_i \sum_{j=1}^{4} \left(a_{ij} \frac{t^j}{j} - \frac{a_{i5}}{t} + a_{i6}\right) \qquad \text{(A-6)}$$

$$c_p = \frac{1}{M} \sum_{i=1}^{6} x_i \sum_{j=1}^{4} \left(a_{ij} t^{j-1} + \frac{a_{i5}}{t^2}\right) \qquad \text{(A-7)}$$

$$c_\phi = \frac{1}{M} \sum_{i=1}^{6} \frac{\partial x_i}{\partial \phi} \sum_{j=1}^{4} \left(a_{ij} \frac{t^j}{j} - \frac{a_{i5}}{t} + a_{i6}\right) -$$

$$- \frac{\partial M/\partial \phi}{M^2} \sum_{i=1}^{6} x_i \sum_{j=1}^{4} \left(a_{ij} \frac{t^j}{j} - \frac{a_{i5}}{t} + a_{i6}\right) \qquad \text{(A-8)}$$

The coefficients a_{ij} are obtained by curve fitting JANAF table data to the above functional form. The values of a_{ij} are given in Table A-2. The resultant c_p is in cal/g-K, while h and c_ϕ are in kcal/g.

Since the cylinder contents are being treated as a mixture of non-reacting ideal gases, the density of the mixture is given by

TABLE A-1

Burned Gas Composition under 1000 K

i	Species	x_i (moles/mole O_2 reactant)	
		$\phi \leq 1$	$\phi > 1$
1	CO_2	$\varepsilon\phi$	$\varepsilon\phi - C$
2	H_2O	$2(1-\varepsilon)\phi$	$2(1-\varepsilon\phi) + C$
3	CO	0	C
4	H_2	0	$2(\phi-1) - C$
5	O_2	$1-\phi$	0
6	N_2	ψ	ψ
	Sum	$(1-\varepsilon)\phi + 1 + \psi$	$(2-\varepsilon)\phi + \psi$

Source: Ref. [49]

TABLE A-2

Coefficients for Polynomial Fit to Thermodynamic Properties

Coefficients for 100 K < T ≤ 500 K:

i	Species	a_{i1}	a_{i2}	a_{i3}	a_{i4}	a_{i5}	a_{i6}*
2	CO_2	4.7373	16.653	-11.232	2.8280	.006767	-93.75793
3	H_2O	7.8097	-.20235	3.4187	-1.1790	.001436	-57.08004
3	CO	6.9739	-.82383	2.9420	-1.1762	.0004132	-27.19597
4	H_2	6.9919	.16170	-.21821	.29682	-.016252	-.118189
5	O_2	6.2957	2.3884	-.031479	-.32674	.004359	.103637
6	N_2	7.0922	-1.2958	3.2069	-1.2022	-.0003458	-.013967

Coefficients for 500 K < T ≤ 6000 K:

i	Species	a_{i1}	a_{i2}	a_{i3}	a_{i4}	a_{i5}	a_{i6}*
1	CO_2	11.940	2.0886	-.47029	.037363	-.58945	-97.1418
2	H_2O	6.1391	4.6078	-.93560	.066695	.033580	-56.62588
3	CO	7.0996	1.2760	-.28775	.022356	-.15987	-27.73464
4	H_2	5.5557	1.7872	-.28813	.019515	.16118	.76498
5	O_2	7.8658	.68837	-.031944	-.0026870	-.20139	-.893455
6	N_2	6.8078	1.4534	-.32899	.025610	-.11895	-.331835

* picked to give enthalpy datum at 0 K

Source: Ref. [49]

C-2

$$\rho = \frac{p}{R_o T}\bar{M} \tag{A-9}$$

where

R_o = the universal gas constant (1.9869 cal/mole-K)

and $\bar{M}$, the average molecular weight of the mixture, is given by

$$\begin{aligned} \bar{M} &= M/((1 - \varepsilon)\phi + 1 + \psi) \qquad \phi \leq 1 \\ \bar{M} &= M/((2 - \varepsilon)\phi + \psi) \qquad \phi > 1 \end{aligned} \tag{A-10}$$

Then, the partial derivatives of the density with respect to temperature, pressure, and equivalence ratio are given by

$$\frac{\partial \rho}{\partial T} = -\frac{\rho}{T} \tag{A-11}$$

$$\frac{\partial \rho}{\partial p} = \frac{\rho}{p} \tag{A-12}$$

$$\frac{\partial \rho}{\partial \phi} = \frac{\partial \rho}{\partial \bar{M}} \frac{\partial \bar{M}}{\partial \phi} = \frac{\rho}{\bar{M}} \frac{\partial \bar{M}}{\partial \phi} \tag{A-13}$$

When the temperature of the cylinder contents is above 1000 K, their properties are calculated with allowance for chemical dissociation, according to the calculation method described in [50]. This is an approximate method based on curve fitting data obtained from detailed thermochemical calculations [30] to a functional form obtained from a consideration of carbon air combustion. Although species concentrations within the burned gases are not calculated, the bulk thermodynamic properties needed for cycle analysis are accurately determined.

APPENDIX B

Thermodynamic Data for Fuel Vapor

In the computer engine simulation code, the fuel vapor enthalpy is modelled by a polynomial of the form

$$H(T) = A_1 t + A_2 \frac{t^2}{2} + A_3 \frac{t^3}{3} + A_4 \frac{t^4}{4} - \frac{A_5}{t} + A_6 \qquad \text{(B-1)}$$

where $t = T/1000$, T is the temperature in Kelvins, and the units of H(T) are kcal/gmole.

The value of A_6 for a particular fuel depends on the datum at which the elements C(graphite), H_2, O_2 and N_2 are assigned zero enthalpy. Using a datum of 298 K, the coefficients A_i were obtained for fuel $C_{10.84}H_{18.68}$ by curve fitting table data from Rossini et al [52] to the above functional form. The values of A_i for various hydrocarbon fuels, including #2 Diesel fuel, are given in Table B-1.

Our thermodynamic property computer codes, however, use a 0K datum. To convert to a 0K datum, a correction term A_8 must be added to the enthalpy given by (E-1) to account for the enthalpy difference of C and H_2 between 0 and 298 K. Using data from the JANAF Tables [53],

$$A_8 = n(H^o_0 - H^o_{298})_c + \frac{m}{2}(H^o_0 - H^o_{298})$$

$$= 10.84 \times 0.252 + \frac{18.68}{2} \times 2.024 = 21.636 \text{ kcal/gmole}$$

TABLE B-1

Coefficients for Polynomial Fit
to Fuel Vapor Data from 300 to 1500 K

Fuel	A_1	A_2	A_3	A_4	A_5	A_6
$C_{12}H_{26}$	-2.2294	277.8[illegible]	-157.08	34.555	0.1970	-79.304
$C_{13}H_{28}$	-2.1801	300.14	-169.86	37.398	0.2105	-85.098
$C_{10}H_{20}$	-12.482	244.84	-142.04	31.844	0.0474	-56.788
$C_{11}H_{22}$	-13.607	270.54	-158.25	35.806	0.0986	-62.192
$C_{10}H_{14}$	-5.7610	196.29	-118.07	27.238	-.0483	-9.5171
$C_{11}H_{16}$	-4.8244	215.96	-128.28	29.245	-.0630	-15.586
Diesel Fuel						
$C_{10.84}H_{18.68}$	-9.1063	246.97	-143.74	32.329	0.0518	-41.166

Source: Ref. [52]

APPENDIX C

Transport Properties

The heat transfer correlations relate the heat transfer coefficient to the Reynolds and Prandtl numbers and the thermal conductivity. The calculation of the heat transfer rates will therefore require values for the viscosity and the Prandtl number (from which the thermal conductivity can be obtained). We have used the approximate correlations for the viscosity and the Prandtl number of hydrocarbon-air combustion products developed by Mansouri and Heywood [51].

The NASA equilibrium program [30] was used to compute the viscosity of hydrocarbon-air combustion products as a function of temperature, T, equivalence ratio, ϕ, and pressure p. It was shown that the viscosity of the combustion products was satisfactorily correlated by a power-law based on air viscosity data, corrected for the effect of equivalence ratio, i.e.,

$$\mu_{prod}\ [kg/ms] = 3.3\times10^{-7} T^{0.7}/(1 + 0.027\phi) \qquad (C\text{-}1)$$

for $500\ K \leq T \leq 4000\ K$ and $0 \leq \phi \leq 4$

Note that the viscosity of the combustion products is independent of the pressure.

The equilibrium Prandtl number of hydrocarbon-air combustion products was also calculated over the above ranges of temperature, pressure, and equivalence ratio. Using a second order polynomial of γ to curve fit the above data, it was shown that the following correlation for lean ($\phi < 1$) mixtures predicted values in good agreement (within 5%) with the data, i.e.,

$$Pr = 0.05 + 4.2(\gamma - 1) - 6.7(\gamma - 1)^2 \qquad (C\text{-}2a)$$

for $500\ K \leq T \leq 4000\ K$ and $\phi \leq 1$

For rich mixtures ($\phi > 1$), a reasonable fit (less than 10% error) to the equilibrium Prandtl number values calculated with the NASA program was found to be the following:

$$Pr = [0.05 + 4.2(\gamma - 1) - 6.7(\gamma - 1)^2]/[1 + 0.015\times10^{-6}(\phi T)^2]$$

for $2000\ K \leq T \leq 3500\ K$ and $1 < \phi \leq 4$ (C-2b)

APPENDIX D

Linearization of Total Heat Transfer Rate at the Gas/Wall Interface

The total instantaneous heat transfer rate, convective and radiative, per unit area, to the combustion chamber walls is given by

$$\dot{Q}_w = \dot{Q}_c + \dot{Q}_r \tag{D-1}$$

where $$\dot{Q}_c = h(T_g - T_w) \tag{D-2}$$

and $$\dot{Q}_r = k_r(T_r^4 - T_w^4) \tag{D-3}$$

where the symbols used have the same meaning as in Section 6.4.

The radiative heat transfer can be expressed as

$$\dot{Q}_r = k_r(T_r^4 - T_g^4) + k_r(T_g^4 - T_w^4) \tag{D-4}$$

or alternatively as

$$\dot{Q}_r = k_r \frac{(T_r^4 - T_g^4)}{T_g - T_w}(T_g - T_w) + k_r(T_g^3 + T_g^2T_w + T_gT_w^2 + T_w^3)(T_g - T_w) \tag{D-5}$$

Combining equations (D-1), (D-2) and (D-5), the total instantaneous heat transfer rate per unit area can be expressed in linear form as

$$\dot{Q}_w = h_{eff}(T_g - T_w) \tag{D-6}$$

where h_{eff} is an effective linearized heat transfer coefficient defined as

$$h_{eff} = h + k_r\left(T_g^3 + T_g^2T_w + T_gT_w^2 + T_w^3 + \frac{T_r^4 - T_g^4}{T_g - T_w}\right) \tag{D-7}$$

1. Report No.	2. Government Accession No.	3. Recipient's Catalog No.
NASA CR-174971		

4. Title and Subtitle	5. Report Date
A Computer Simulation of the Turbocharged Turbo-compounded Diesel Engine System: A Description of the Thermodynamic and Heat Transfer Models	September 1985
	6. Performing Organization Code
7. Author(s)	8. Performing Organization Report No.
Dennis N. Assanis, Jack E. Ekchian, Rick M. Frank, and John B. Heywood	
	10. Work Unit No.
9. Performing Organization Name and Address	11. Contract or Grant No.
Sloan Automotive Laboratory Massachusetts Institute of Technology Cambridge, Massachusetts 02139	NAG 3-340
	13. Type of Report and Period Covered
12. Sponsoring Agency Name and Address	Contractor Report
U.S. Department of Energy Office of Vehicle and Engine R&D Washington, D.C. 20585	14. Sponsoring Agency Code Report No. DOE/NASA/0340-1

15. Supplementary Notes

Final report. Prepared under Interagency Agreement DE-A101-80CS50194. Project Manager, George M. Prok, Propulsion Systems Division, NASA Lewis Research Center, Cleveland, Ohio 44135.

16. Abstract

A computer simulation of the turbocharged turbocompounded direct-injection diesel engine system has been developed in order to study the performance characteristics of the total system as major design parameters and materials are varied. Quasi-steady flow models of the compressor, turbines, manifolds, intercooler, and ducting are coupled with a multi-cylinder reciprocator diesel model, where each cylinder undergoes the same thermodynamic cycle. The master cylinder model describes the reciprocator intake, compression, combustion and exhaust processes in sufficient detail to define the mass and energy transfers in each sub-system of the total engine system. Appropriate thermal loading models relate the heat flow through critical system components to material properties and design details. From this information, the simulation predicts the performance gains, and assesses the system design trade-offs which would result from the introduction of selected heat transfer reduction materials in key system components, over a range of operating conditions.

17. Key Words (Suggested by Author(s))	18. Distribution Statement
Diesel engines, Turbocompounding, Low heat-rejection engines, Ceramics in engines	Unclassified - unlimited STAR Category 85 DOE Category UC-96

19. Security Classif. (of this report)	20. Security Classif. (of this page)	21. No. of pages	22. Price*
Unclassified	Unclassified	109	A06

*For sale by the National Technical Information Service, Springfield, Virginia 22161